LCC-0104
October 2002

Linear Collider Collaboration Tech Notes

Beamstrahlung Photon Load on the TESLA Extraction Septum Blade

Andrei Seryi

Stanford Linear Accelerator Center
Stanford, CA 94309, USA

Abstract: This note describes work performed in the framework of the International Linear Collider Technical Review Committee [1] to estimate the power load on the TESLA extraction septum blade due to beamstrahlung photons. It is shown, that under realistic conditions the photon load can be several orders of magnitude higher than what was estimated in the TESLA TDR [2] for the ideal Gaussian beams, potentially representing a serious limitation of the current design .

Beamstrahlung Photon Load on the TESLA Extraction Septum Blade

ANDREI SERYI

STANFORD LINEAR ACCELERATOR CENTER

LCC-Note-0104

October 2002

Abstract

This note describes work performed in the framework of the International Linear Collider Technical Review Committee [1] to estimate the power load on the TESLA extraction septum blade due to beamstrahlung photons. It is shown, that under realistic conditions the photon load can be several orders of magnitude higher than what was estimated in the TESLA TDR [2] for the ideal Gaussian beams, potentially representing a serious limitation of the current design.

1 Introduction

In the TESLA linear collider design [2], the outgoing disrupted beams (charged and neutral) share the same beamline with the incoming beam for at least 50 m past the IP. The disrupted primary beam is deflected first by combined electrostatic and magnetic separator (which does not deflect the incoming beam) and then by a septum magnet. Beam losses on the beamline components from the disrupted beam, and from secondary and neutral beams, need to be sufficiently small.

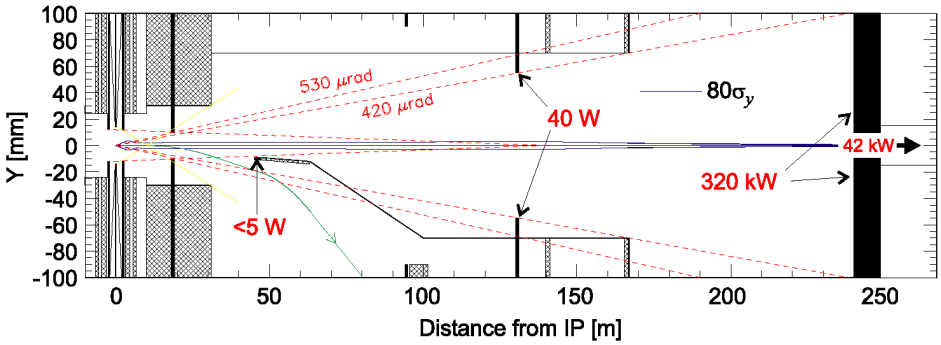

Figure 7.6.4: *Vertical layout of the final transformer region. The beamstrahlung power levels on the collimators are for the* $E_{cm} = 500\,GeV$ *machine.*

Figure 1: Picture from the TESLA TDR. The power levels correspond to the ideal Gaussian beams with nominal parameters.

In particular, excessive power deposition from beamstrahlung photons need to be avoided. Figure.1 is reproduced from the TESLA TDR [2] and shows that the beamstrahlung radiation is transported to the main dump hall essentially without losses (less than 50 W out of 360 kW total power). In particular, only less than 5 W is nominally deposited on the septum blade.

The quoted power levels apparently correspond to ideal Gaussian beams with nominal parameters. It was pointed out [3] that in more realistic conditions (e.g. with beam jitter due to ground motion and vibration, and with some emittance growth due to misalignments) the photon loads may increase significantly.

Preliminary studies have confirmed [4] that in non-ideal conditions, where the delivered luminosity is still about 75% of nominal, the photon load on the septum blade may reach 1500 to 2500 W on average. The total radiated power was also higher for the non-ideal beam: about 500 kW instead of 360 kW.

In this note, the beamstrahlung photon loads on the TESLA extraction septum blade are evaluated more systematically: with more cases studied and with better statistics. The earlier preliminary results [4] are also included for consistency.

Dependence on parameters is also studied and presented below. In particular, the following cases are considered: the low disruption TESLA parameter set (see [1], TESLA project description), intended to halve the disruption parameter D_y to reduce sensitivity to "banana effect"; a commissioning mode, when the vertical beam size is larger than the desired value; and the TESLA 800 GeV CM parameters.

2 An Ideal Gaussian Beam Case

To evaluate the photon power load on the septum blade, it is essential to perform full beam-beam simulations. The program GUINEA-PIG [5] was used for this purpose. Beamstrahlung photons, generated during collision, were stored and then their angular distribution was analyzed to find the amount of total photon power on the septum. This procedure is illustrated by Fig.2 where collision of ideal Gaussian beams with nominal TESLA parameters is shown together with the resulting spatial distribution of beamstrahlung photons in different projections as well as the angular distribution of the photon energy (in GeV per mrad per bunch crossing). The septum blade is defined as $y = 9$ mm to $y = 11$ mm at 45m from the IP, or, in terms of the angles, $0.2 \leq y' \leq 0.2444$ mrad. The power loads are obtained by integrating the total energy of all photons in this angular range.

For the ideal Gaussian beam with nominal TESLA parameters, (Fig.2) the losses on the blade were found to be ~ 3.5 W, and the total photon power was found to be ~ 360 kW, in good agreement with TDR [2]. However, this agreement could only be achieved if a large number of macro-particles were used in GUINEA-PIG to represent the beam – in this particular case 300K macro-particles were used which is about ten times larger than what is typical. Considering this example with the ideal beams (Fig.2), we need to note that collisions of the beams remain symmetrical and there is almost no evidence of the beam-beam instability in spite of the large vertical disruption parameter (which is larger than 20). This is because, for the large number of macro-particles, statistical offsets of the beam are small and instability is suppressed. Taking into account that at the location of the blade the photon distribution from the ideal beam is rapidly decreasing, and the septum is placed just at the cut-off, one can already conclude that there is not much of a margin in the present design and more realistic conditions should be investigated.

3 Integrated Simulations of Realistic Conditions

Realistic evaluation of the photon load on the septum blade requires integrated consideration of the whole machine, with account for various imperfections and errors (static and dynamic) happening along the beamline. Integrated simulations of TESLA have been performed using the MAT-LIAR code [6] which includes the LIAR code for tracking in the linac, the DIMAD code for tracking in bunch compressor and beam delivery, and GUINEA-PIG for full beam-beam simulations, all encompassed by the power and flexibility of MATLAB.

A beam is tracked from the beginning of the linac to the IP. The beamline elements may have both static and dynamic misalignments (ground motion and vibration). Three ground motion models **A**, **B** and **C** (quiet, moderate and noisy) were typically used to represent the dynamic misalignments. The ground motion model **A** is based on measurements performed in the LEP tunnel, the model **B** is based on measurements performed at SLAC, and the ground motion model **C** is based on measurements performed at DESY. Additional vibration of the final doublet (FD) can also be included in simulations [10, 11]. Though multi-bunch simulations can be performed in MAT-LIAR, to minimize computing time and because multi-bunch effects are normally not of a particular importance for TESLA and could be ignored, only one bunch is tracked per pulse, to represent the entire train. Two linacs and beam delivery systems (e- and e+ beamlines) are tracked simultaneously. Identical optics is used for e- and e+ parts, however an increase of the e- beam energy spread by 0.14% in the TESLA positron production wiggler is taken into account.

Two different models of the TESLA fast intratrain IP beam-beam feedback have been simulated. In the first (simplified) feedback model, the average position offset of the beams at the IP is subtracted before the beams collide. This model would correspond to a BPM based IP feedback. In the second feedback model (feedback with full optimization within the train) the average offsets (position and angle in this case) are subtracted, then the vertical beam separation and the vertical angle are optimized to maximize the luminosity for the rest of the train. This feedback assumes that a fast and accurate luminosity monitor exists. In this way, each calculated pulse corresponds to a train with assumptions that all bunches in the train are equally well corrected by the feedback. The beamstrahlung photons are calculated for

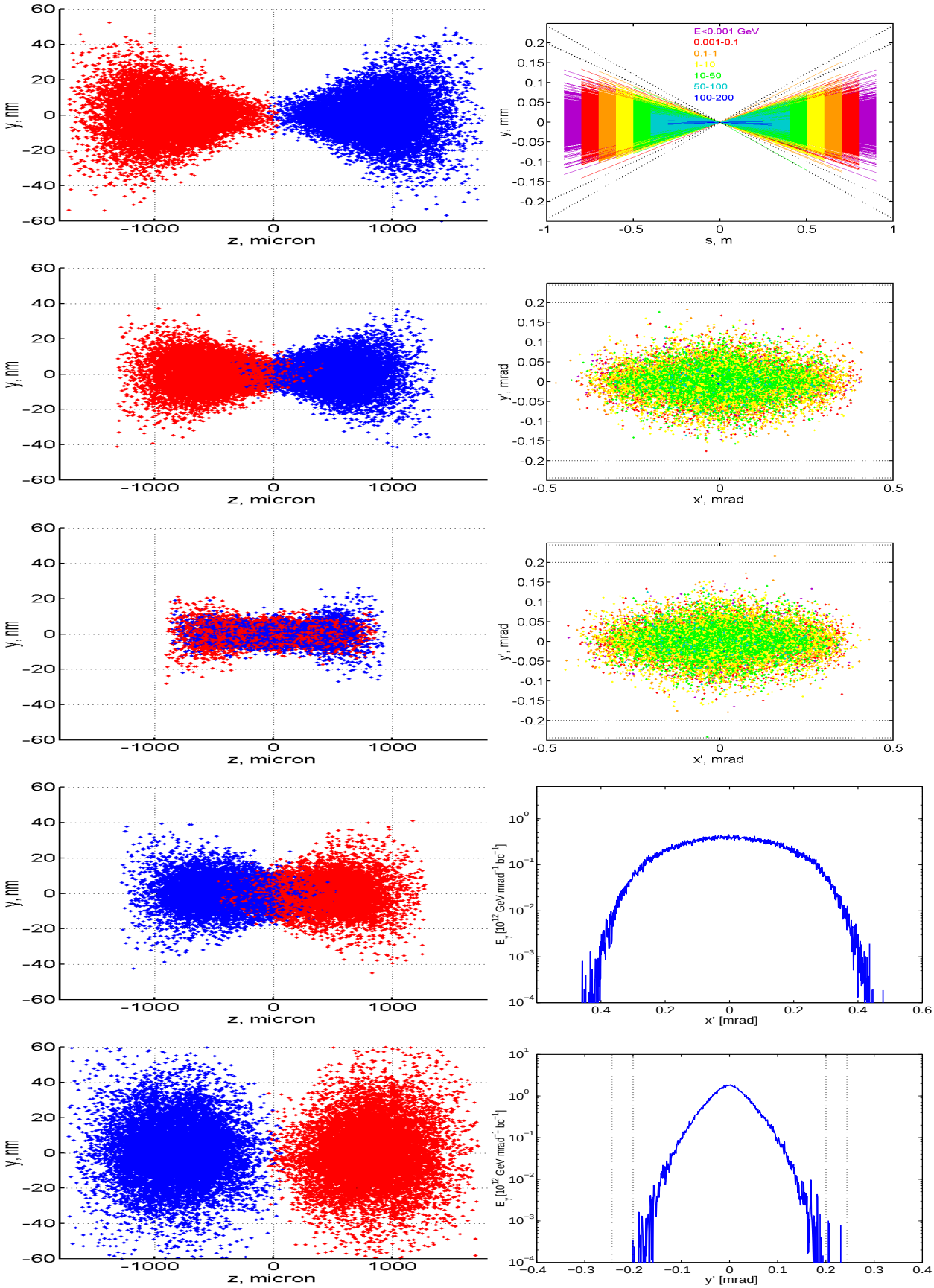

Figure 2: Collision of ideal Gaussian beams with nominal TESLA parameters, several consecutive snap-shots (left). Spatial distribution of beamstrahlung photons in *sy* and $x'y'$ (for each beam) projections (photon energy is color coded), and distribution of photon energy versus x' and y' (right). Dashed lines show angular location of the septum.

the beams with feedback already applied, and the calculated losses on the septum blade are therefore equivalent to the average over the train (ignoring bunch-to-bunch position jitter in the train).

In order to estimate the power load on the blade due to the initial part of the train, where the intratrain feedback is sweeping fast to bring the beams into collision, the beam-beam simulations were also performed without applying the IP feedback. The losses on the blade in this case must be weighted by the fraction of the train not in collision, taking into account the feedback convergence speed. For example, if one assumes that the intratrain feedback will bring the trains into collision within the first 5 bunches, the contribution of those 5 bunches to the total power load will be about 5/2820 of the calculated losses, where 2820 is the number of bunches in the TESLA 500 GeV CM train.

In this way, the beginning of the train (which may have significant offset), and the majority of the train (which is brought into collision by the fast intratrain feedback), are considered separately. The total average power on the septum blade is estimated by adding these two numbers weighted appropriately.

Since the up and down directions are interchangeable in simulations, and the non-ideal beam can be asymmetrical, both directions were checked and compared, in terms of the power load on septum, for both e+ and e- beams.

4 Realistic Cases Considered

It is essential that such simulations are performed for machines with realistic misalignment of beamline elements (accelerating structures and quadrupoles) and with realistic beam jitter driven, in particular, by ground motion and vibration. The initial misalignments have been chosen in such a way that the machine produces luminosity close to the nominal (which is assumed to be $34.5*10^{33}$ $cm^{-2}s^{-1}$). This approach will allow, in particular, consideration of realistic emittance growth in the linac and realistic beam-beam effects.

Several different cases were studied.

- **Case 1.** A single non-ideal TESLA machine was constructed by assuming that linac has 200 micron random misalignments of accelerating structures. Emittance growth in the linac was corrected by transversely offsetting some accelerating structures. Ground motion model **C**, and additional vibration of the final doublet were applied. The simplified model for the intratrain IP feedback was used. Initial luminosity of this machine was approximately equal to the nominal. This is the same case as considered in [4] and it is reproduced here for consistency.

- **Case 2.** One hundred non-ideal machines was constructed by introducing a set of errors to the linac part of a perfect machine and then applying one-to-one correction to the linac to bring the machine back to approximately nominal luminosity. The following three types of errors were used: BPM-to-quad offset σ_{BPM}, RF structure offset w.r.t. survey line σ_{RF}, RF structure tilts w.r.t. survey line σ_{RFtilt} (all uncorrelated). The values used were: (σ_{BPM}, σ_{RF}, σ_{RFtilt}) = (25μm, 600μm, 300μrad). The intratrain IP feedback with full optimization was used to bring the luminosity of these machines close to the nominal. Assuming that such feedback is applied, and there are no other dynamic misalignments, the first collision was used to determine photon load for all hundred machines.

- **Case 2a.** For one particular machine built as in Case 2, ground motion model **C** was applied and the intratrain IP feedback with full optimization was used for 256 consecutive trains (which corresponds to 51 s at 5 Hz TESLA repetition rate). The initial luminosity of this particular machine was equal to the nominal.

- **Case 2b.** The same as case 2a, but additional vibration noise of the final doublet was included.

- **Case 3a.** The non-ideal machine was constructed in the same way as in the case 2, but a different error seed was chosen. The ground motion seed was the same as in the case 2a. The initial luminosity of this machine was equal to about 80% of the nominal.

- **Case 3b.** The same as case 3a, but additional vibration of the final doublet was included.

In all these simulations, only the IP feedback was taken into account for dynamic corrections. No other feedback or orbit correction, either in the linac or in the beam delivery, was applied. In principle, the orbit correction in the beam delivery should be taken into account, since its absence results in a slow decrease of the luminosity which is already noticeable after approximately hundred pulses.

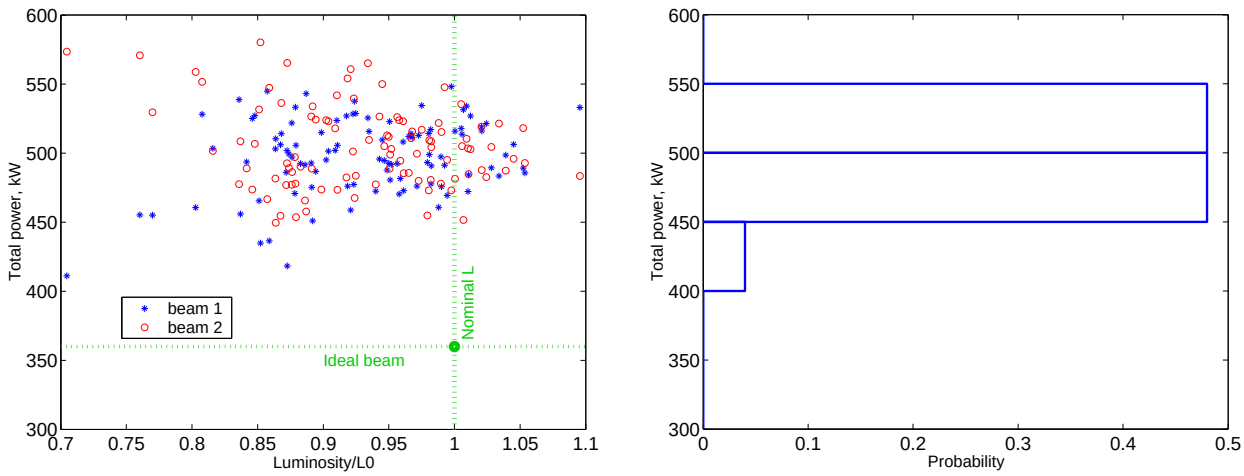

Figure 3: One hundred non-ideal machines (Case 2). Total beamstrahlung power versus luminosity of the first collision (left plot) and probability distribution of the power (right plot) for all machines considered.

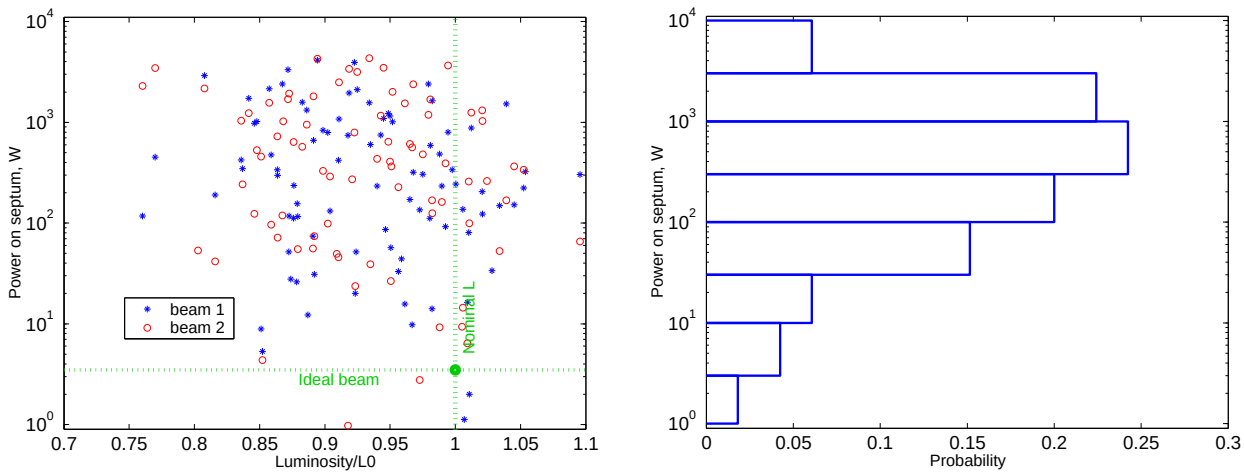

Figure 4: One hundred non-ideal machines (Case 2). Beamstrahlung power on septum versus luminosity of the first collision (left plot) and probability distribution of the power (right plot) for all machines considered. Note the logarithmic scale for power on the septum blade.

5 Results and Discussion

The results for **Case 1** (considered in [4] and quoted in [1]) are presented in Fig.12-16. Fig.12 shows the beam position at the IP before the simplified IP feedback is applied, and the luminosity after feedback is applied. (All pictures presented for case 1 show pulses 140 to 170 of the total 256 calculated. This corresponds to a sequence of particle data files saved in this simulation). The average luminosity for this sequence of pulses is about 75% of nominal. Fig.12 also shows that, for this sequence of pulses, the rms of the beam position difference before feedback was about 37nm, which is still small compared with the quoted in TDR capabilities of the fast intratrain feedback.

The total photon power for the non-ideal beam is shown in Fig.13. One can see that the total photon power is about 500 kW, i.e. about 50% higher than for the ideal Gaussian beams. Without IP feedback, the total power is about 650 kW. The photon distributions for the non-ideal beam after being brought into collision by feedback are shown in Fig.15. These distributions are wider than for the ideal beam (especially in y), causing the losses on the blade to be about 1500 - 2500 W on average depending on the beam (see Fig.14, left plot). This figure also shows that the losses fluctuate significantly from pulse-to-pulse. The observed losses are hundreds times higher than what was stated for the ideal beams. Again, these losses are averaged over many trains, and therefore they are relevant.

The photon distributions for the non-ideal beam not yet brought into collision is even wider and also asymmetrical, see Fig.16. The Fig.14 (right plot) shows that for the beginning of the train the instantaneous losses on the septum blade are about 10 times higher than for the majority of the train (about 8 kW for one beam, and 58 kW for another in this case). Assuming that the feedback brings the beams into collision within the first 5 bunches, as it is simulated in [9], the contribution of the beginning of the train to the total power is about $5/2820 * 58$ kW ~ 100 W, still small in comparison with the rest of the train. Therefore, higher instantaneous loads from the beginning of the train are less

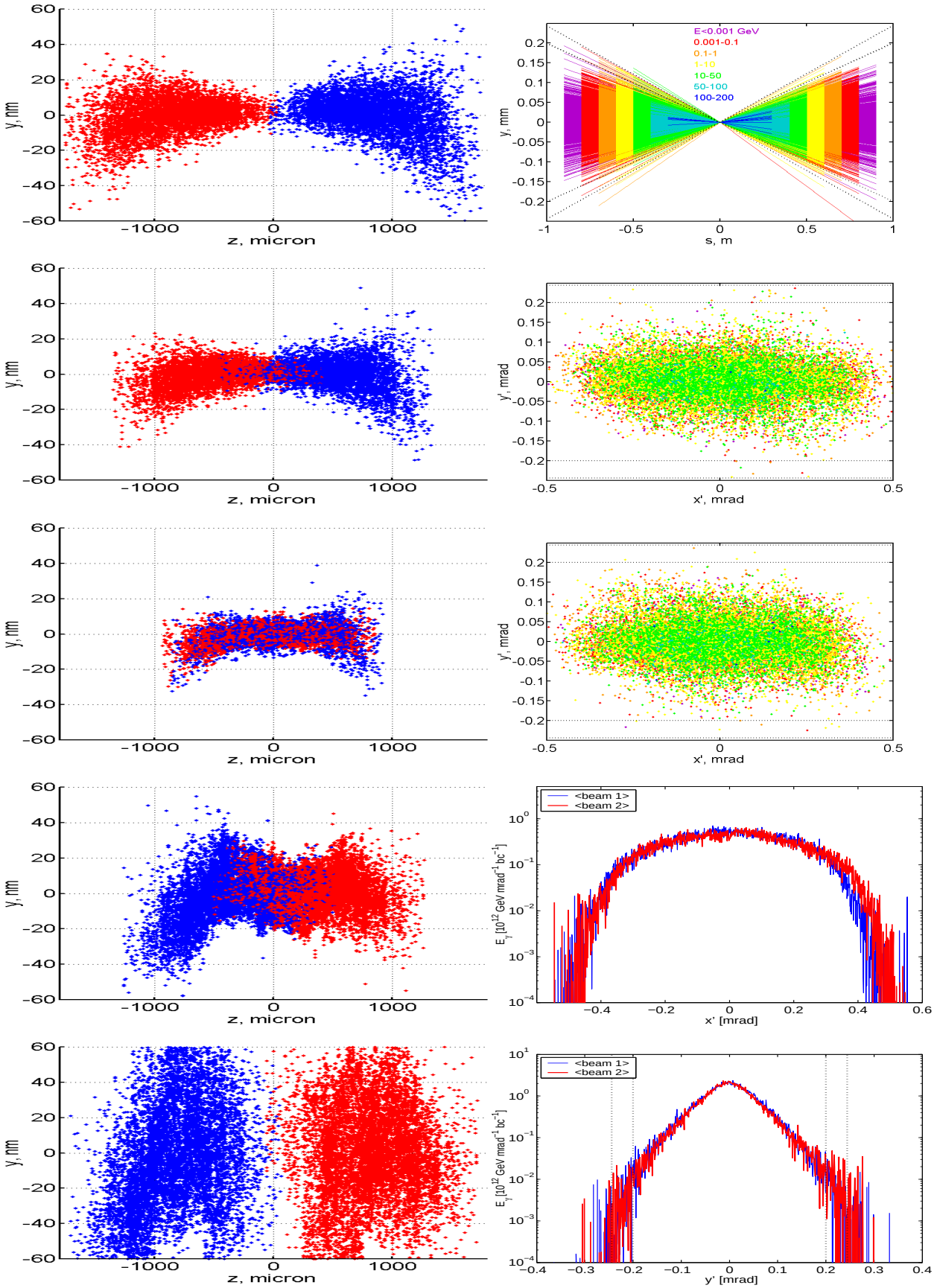

Figure 5: An example with non-ideal TESLA beams. Collision, several consecutive snap-shots (left). Spatial distribution of beamstrahlung photons and angular distribution of photon energy (right). For this particular collision the luminosity was 97.5%, photon load on septum reached 0.48 kW.

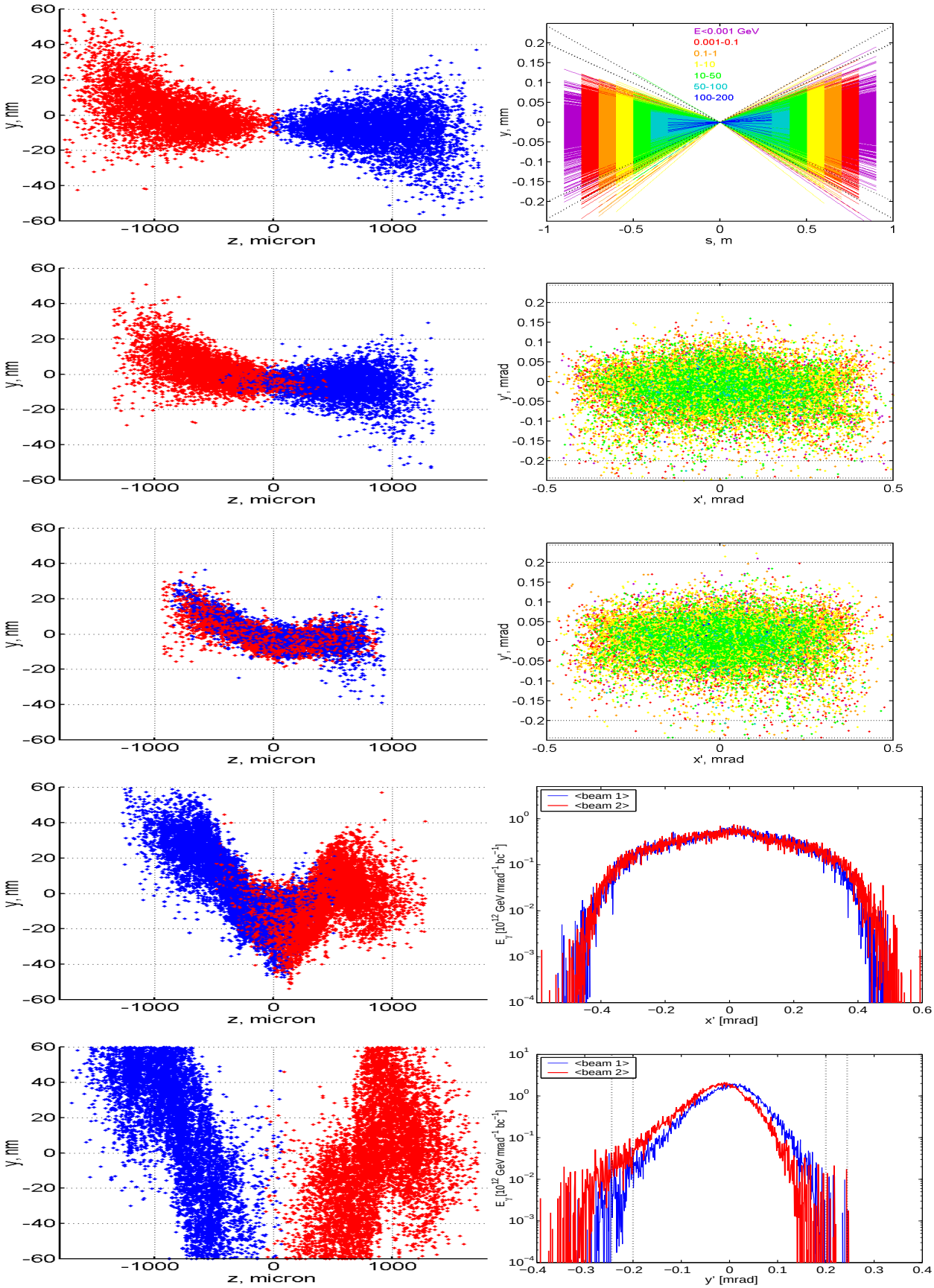

Figure 6: An example with non-ideal TESLA beams, with more pronounced banana-shape. Collision, several consecutive snap-shots (left). Right pictures show spatial distribution of beamstrahlung photons and angular distribution of photon energy (right). For this collision luminosity was 100.5%, photon load on septum reached 3 kW.

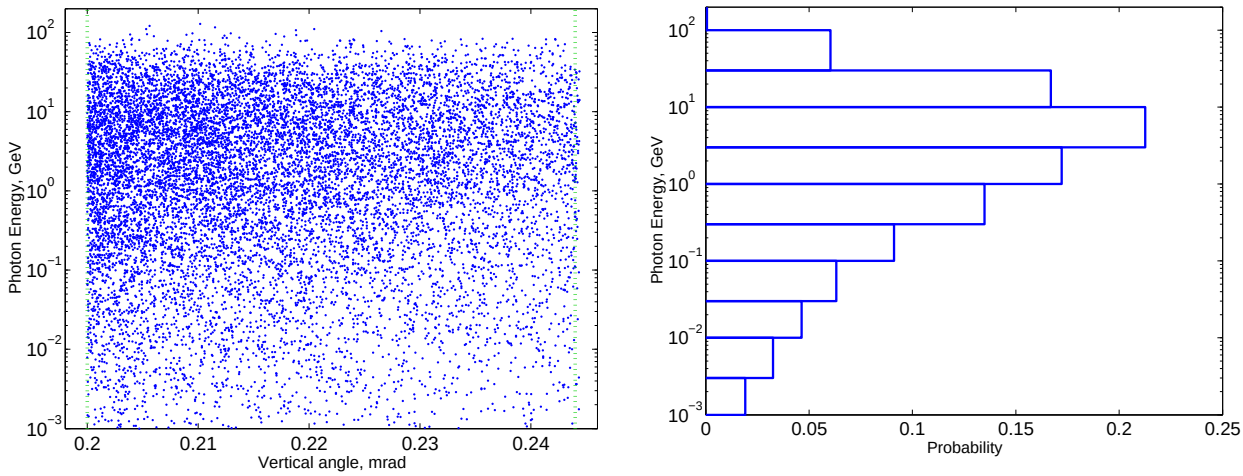

Figure 7: Photons coming onto one of the blades (Case 2a). Photon energy versus vertical angle (left plot) and probability distribution of the photon energy (right plot) for the first 256 pulses.

of a problem. This conclusion assumes, however, that the intratrain feedback is not allowed to fail (or to perform less than perfectly) even when commissioning, which may make it very difficult to tune the final focus and setup the IP feedback.

Results for one hundred machines considered in the **Case 2** are presented in Fig.3 and 4. Fig.3 shows luminosity of the first collision of each machine versus total beamstrahlung power. About a half of these one hundred machines have luminosity within 5% of the nominal. As in the previous case, the most probable total photon power is about 500 kW. Photon power load on septum, as a function of luminosity, is shown in Fig.4, together with probability distribution of the photon power on the septum blade. One can see that there is no significant correlation between luminosity and either the total power or the power load, though the power load is generally lower if luminosity is higher (at least in the luminosity range from 0.95 to 1.05 of the nominal). Probability to have photon load of 5 W, as in Fig.1, is less than several percents. With probability of 30% the power load on septum will exceed 1 kW, and with probability higher than 50% it will exceed 300 W.

These high power loads on the septum are mostly due to the beam-beam instability, occurring in the colliding beams because of the high disruption parameter and driven by small initial offsets or deformations in the bunch shape (banana-like beams), which also often results in asymmetrical distribution of outgoing photons. A couple of examples of collisions of non-ideal beams, together with photon distributions, are shown in Fig.5 and 6. In these two examples the initial beam shapes are different and far from ideal (in the last case the beams and outgoing photons are quite asymmetrical) but the beam shapes match each other in such a way that the development of instability is delayed and partly suppressed so that it does not cause decrease of luminosity.

Results for **Case 2a** are presented in Fig.7 and Fig.17-23. Qualitatively, the results are similar to the Case 1. Some particular comments are given below.

Fig.7 shows probability distribution of the photon energy for the photons coming onto one of the septum blades averaged over the first 256 pulses of this case. One can see that about 5% of the hitting photons have energy higher than 30 GeV and about 50% of photons have energy higher than 3 GeV. Fig.17 shows that the luminosity (after feedback with full maximization) starts from the nominal value and slowly decreases to about 65% to the end of the sequence. This decline of luminosity is caused by growing aberrations in the beam delivery, and could be avoided if orbit correction in the beam delivery were applied. It is interesting, however, to follow the dependence of the power on the septum blades versus luminosity. One can see that with luminosity about 100% of the nominal the photon power load is about 0.5 kW; with $L \sim 75\%$ the power reaches 1.5-2 kW; and with $L \sim 65\%$ the power reaches 4 kW. One can also see that power loads for e+ and e- beamlines can differ significantly.

Results for **Case 2b** are similar to the previous case. Additional vibration of the final doublet results in larger fluctuations of the luminosity and higher power from the initial part of the train, which is not yet brought into collision by the intratrain IP feedback. This case is presented in Fig.24 to 28.

Results for **Case 3a** are presented in Fig.29-35. The luminosity (after feedback with full maximization) starts from 80% of the nominal value and decreases to about 55% to the end of the sequence. The photon power loads reach 1-3.5 kW at $L \sim 80\%$ and 2-6 kW at $L \sim 55\%$.

The **Case 3b** is qualitatively similar to case 3a. Again, the additional vibration of the final doublet results in larger fluctuations of the luminosity and higher power on the blade for the initial part of the train. Corresponding plots are in Fig.36 to 40.

To summarize, the correlation between the average power load on the septum blade and the luminosity is given in the Table.1. As already mentioned, in these cases the decrease of the luminosity is caused by aberrations in beam delivery system. It appears that these aberrations change the shape of the beams in such a way that these shapes are no longer matched to suppress the beam-beam instability. Increased instability results in lower luminosity and higher photon loads on septum.

Table 1: Approximate relations between the average power loads on the septum blade and luminosity observed in the considered cases. (IP feedback is applied.)

Luminosity	Case 1	Cases 2a,b	Cases 3a,b
100%		0.5 kW	
80%			1-3.5 kW
75%	1.5-2.5 kW	1.5-2 kW	
65%		4 kW	
55%			2-6 kW

Therefore, in general, smaller luminosity corresponds to higher power load on the septum. This would make it especially problematic when the machine is being commissioned and has not yet attained a nominal luminosity.

The correlation of power load and luminosity holds on average and depends on the details of the beam shape. For a given sequence of trains this correlation may be absent. One can see that for case 2a, the power load is uncorrelated with the luminosity in the range of $L = 80\%$ to 100% (Fig.23) and for case 3a the power load is uncorrelated with the luminosity in the range of $L = 60\%$ to 80% (Fig.35). It appears, from this observation, that one cannot use the power load as a signal to maximize luminosity, and vice versa – maximization of the luminosity may not necessarily result in a smaller power loads on septum, at least if the luminosity is within about 20% of the maximum. For a cruder optimization of luminosity, the power load on septum (or a dedicated device, notwithstanding any issues of hardware survivability) can obviously serve as a signal for the feedback which maximize the luminosity, even within a single train, since the power loads for the beam not brought into collision are more than ten times higher than for the beam already brought into collision by a feedback.

6 Dependence on the Ideal Beam Parameters

In this section, we will study dependence of the losses on the ideal beam parameters. We check several standard sets of parameters and also investigate parameters that might be encountered when commissioning. Note that for this parameter study an ideal Gaussian beam was used, calculated with large (300K) number of particles, so that beam-beam instability is suppressed. Therefore, all these results on dependence on parameters are preliminary and need to be augmented by consideration of non-ideal beams.

Three cases of standard parameters are compared below (all for ideal Gaussian beams):

- Standard TESLA 500 GeV CM parameter set
  $\sigma_x^*/\sigma_y^* = 554/5$ nm, $\beta_x^*/\beta_y^* = 15/0.4$ mm, $\sigma_z = 300$ μm, $N = 2 \cdot 10^{10}$
- Alternative TESLA 500 GeV CM parameters with half the vertical disruption parameter D_y, where the sensitivity to the "banana effect" would be reduced (see [1], TESLA Project Description). The bunch length σ_z is halved, 150μm instead of 300μm (this would require a second bunch compressor), the horizontal beta function at the IP is 20 mm instead of 15 mm, and the vertical beta function is 0.3 mm instead of 0.4 mm.
- Standard TESLA 800 GeV CM parameter set
  $\sigma_x^*/\sigma_y^* = 391/2.8$ nm, $\beta_x^*/\beta_y^* = 15/0.4$ mm, $\sigma_z = 300$ μm, $N = 1.4 \cdot 10^{10}$

Results for these cases are shown in Fig.8. One can see that even for the ideal beam, the photon angles are noticeably wider for the alternative 500 GeV parameter set with low D_y than for the standard parameter set, and extend into the angular range of the septum. Power load on septum is about 100 W even for this ideal beam, which can hardly be an advantage of this parameter set. Of course it is possible that when considering non-ideal beams with these parameters, the beam-beam instability will be smaller and will not increase the photon load on the septum.

On the other hand, the situation seems to be better for the 800 GeV parameters. For the ideal beam the photon angles are about half that for 500 GeV beam parameters. Non-ideal beams must be studied for this case as well to verify the conclusions, because D_y is actually larger than for the 500 GeV parameters.

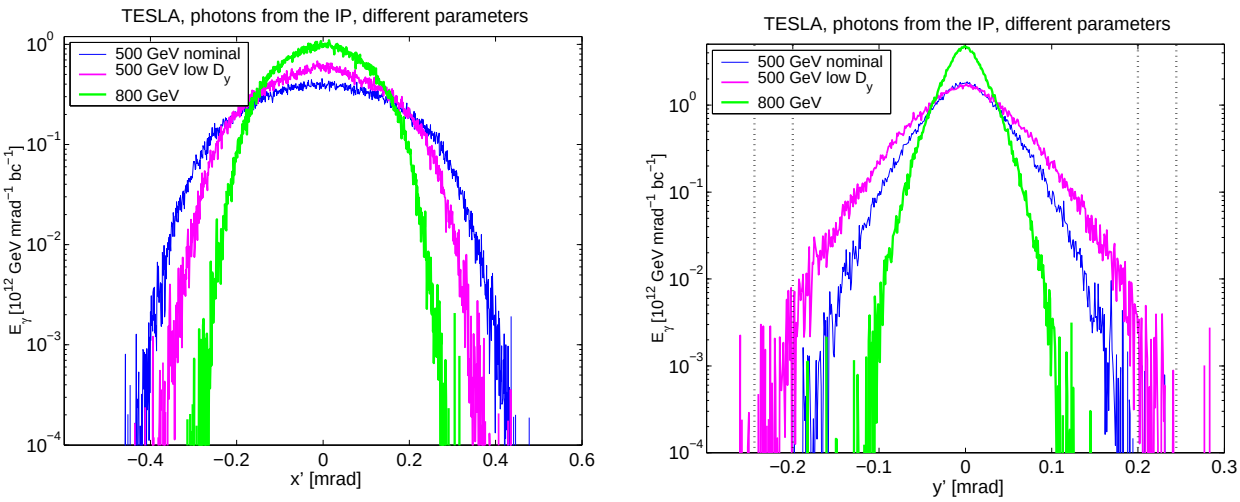

Figure 8: Horizontal (left) and vertical (right) distributions of beamstrahlung photons for the ideal Gaussian beams with different parameters: nominal 500 GeV CM case; alternative 500 GeV CM parameter set with halved disruption parameter D_y (reduced sensitivity to "banana" effect); nominal 800 GeV CM case.

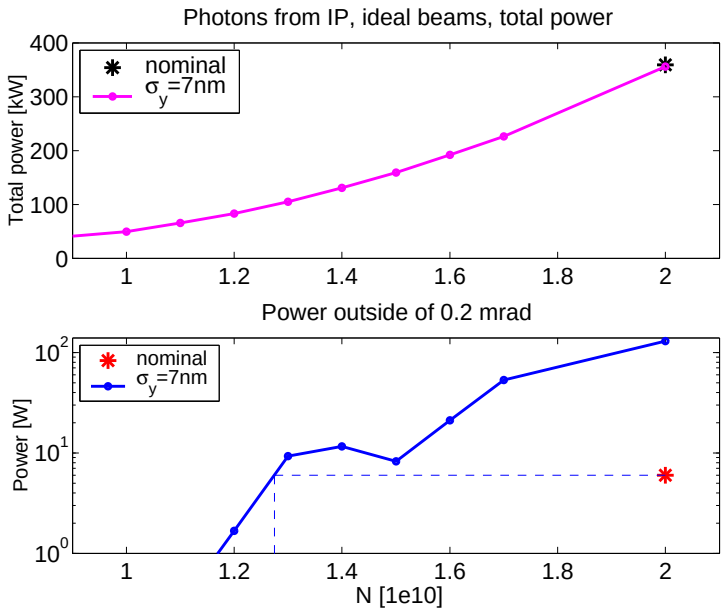

Figure 9: Total power of beamstrahlung photons (top plot) for the ideal beams and power outside y'=0.2 mrad (averaged for negative and positive directions, bottom plot) versus bunch population for nominal 500 GeV CM case and for the 500 GeV CM parameters with larger vertical beam size (7nm instead of nominal 5nm).

It is also important to understand how the photon load would behave towards the end of commissioning, when the beam parameters are close to nominal. Let's consider again the standard 500 GeV case and suppose that all parameters are already nominal, but the vertical beam size is larger (which could be a realistic scenario). Let's assume that the vertical size is $\sigma_y = 7$ nm instead of the nominal 5 nm. One can see from the Fig.9 and Fig.10 that the power load on the septum will increase from about 5 W to about 120 W for $\sigma_y = 7$ nm. (These simulations were also performed for ideal Gaussian beams, so the power numbers are just an indication).

Suppose now that we want to decrease the beam current to reduce the photon load to the same value as observed for the nominal beam. Dependence of the photon power load on the bunch population is shown in Fig.9. One can see that one would need to decrease the current to about $N = 1.3 \cdot 10^{10}$ with respect to the nominal $2 \cdot 10^{10}$, in order to keep the power load at the same level. This would imply that the luminosity would be reduced to $(5/7) * (1.3/2)^2 \approx 30\%$ – a much larger reduction than what one would expect just from the beam size increase.

From this parameter study, where different σ_y, σ_z, N and the beam energy were considered, one could suggest a

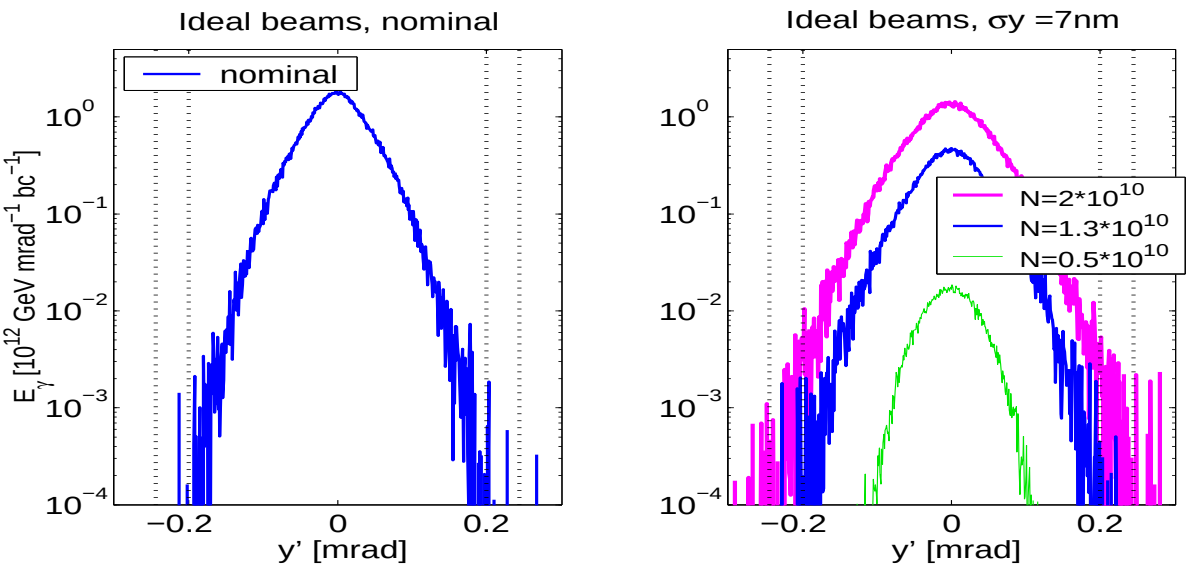

Figure 10: Vertical distributions of beamstrahlung photons for the ideal beams with different parameters: nominal 500 GeV CM case (left plot); 500 GeV CM parameters with larger vertical beam size (7nm instead of nominal 5nm) and smaller bunch population (right plot).

very tentative scaling for the maximal vertical angles of photons (for the ideal Gaussian beams):

$$\Theta_y \sim \sigma_y \, N/\sigma_z$$

Though the total photon power depends on the beam energy, there seems to be no dependence of the maximal photon angle on the beam energy. The scaling of the photon angles on parameters, given above, may not be quite obvious. For example, the disruption angles of particles after beam-beam interaction, as deduced from computer simulations, are given by $\theta_y \approx 0.55 D_y \sigma_y \sigma_z^{-1} (1 + (0.5 D_y)^5)^{-1/6}$ [7] which for large D_y behaves as $\theta_y \approx D_y^{1/6} \sigma_y / \sigma_z$ and almost does not depend on the bunch population N in contrast with the photon angles.

Summarizing, the alternative TESLA parameter set, intended to halve the disruption parameter and reduce sensitivity to "banana effect", would have similar or higher photon loads in comparison with the standard parameters. The problem of photon loads becomes more severe in the commissioning mode, when the vertical beam size is still larger than the desired value. Again, this study of parameter dependence is for ideal beams only, and should be augmented by consideration of non-ideal beams, to account for the effect of beam-beam instability.

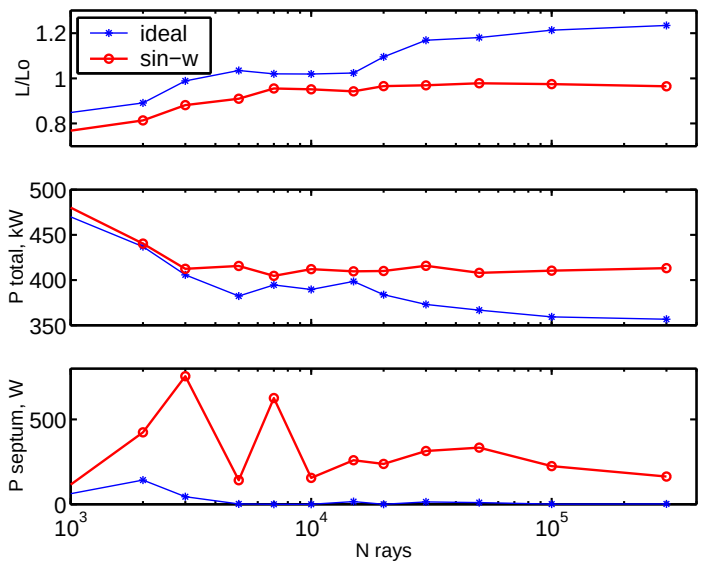

Figure 11: Luminosity, total beamstrahlung power and photon power load on septum versus number of macro-particles per beam used in beam-beam simulations. Ideal Gaussian beam and a beam with artificial small sin-like distortion of the vertical shape.

7 On the accuracy of beam-beam calculations

In all these studies, beam-beam simulations for the non-ideal beams were made with 12K macro-particles per beam. The accuracy of the luminosity and power estimations can be judged from Fig.11. In this case, collisions of an ideal Gaussian beam were compared with collisions of the beams which have small sin-like (or banana-like) distortion of the vertical shape. Such beams were generated with exactly the same shape but with different numbers of macro-particles and then the results were compared. One can see from Fig.11 that with 12K macro-particles representing the non-ideal beam, the accuracy of luminosity and total power estimation is within several percents, and the accuracy of the photon power load on septum estimation is within about 30% which is sufficient.

One can see that for the ideal beam, at least 300K macro-particles are needed to accurately estimate the luminosity and photon power. Note again, that the large number of macro-particles in this case reduces statistical fluctuations in the beam and therefore suppress beam-beam instability. Though studying the ideal beams could be useful, as a necessary first step, such precisely symmetrical beams cannot be realized in practice.

8 What is not included or needs to be studied further

In this note, it is assumed that fast feedback can start immediately from the beginning of the train. The beginning of the train may have an irregular transverse pattern due to high order modes (HOM) that have not yet reached the steady state of HOM excitation. According to the TDR, this pattern is static (reproducible from pulse to pulse) and can be removed by feed-forward correction at the end of the linac. If the start of the fast feedback is delayed with respect to the start of the train, for any reason, the contribution to the photon load on the septum from the beginning of the train will correspondingly increase.

In the simulation of the intratrain feedback the beam position and angles were simply adjusted before beam-beam simulations, and not obtained by change of the corresponding correctors in the beamline. Therefore, any dispersion or other aberrations that could result from these correctors were ignored.

There are studies that suggest thickening the septum magnet blade to 5 mm. This could result in even higher power loads, but perhaps facilitate cooling.

Photon loads on other beamline elements need to be reevaluated.

The multi-bunch effects and in particular the bunch-to-bunch position jitter or shape jitter of the bunches within the train were not taken into account. Effects such as wake fields in the beam delivery collimators, which could enhance beam position jitter [8], were not included either.

Power loads on septum were estimated as simple sum of energy of all hitting photons. Details of interaction with material and survivability of septum (or masks shadowing septum) should be investigated. Other mitigation measures (such as introduction of a horizontal crossing angle), should be evaluated.

9 Conclusion

In imperfect realistic conditions the average beamstrahlung photon power load on the TESLA extraction septum blade can reach the kilowatt level instead of several watts expected for an ideal beam. High photon loads on the extraction septum blade may pose serious limitation of the present design and should be investigated further.

10 Acknowledgements

Studies presented here were performed using the MAT-LIAR code, developed by the NLC Accelerator Physics group, that allowed integrated simulations of the entire linear collider from damping rings to the IP taking into account various imperfections.

References

[1] International Linear Collider Technical Review Commitee (ILC-TRC), 2002; ILC-TRC Report, to be published.

[2] TESLA Technical Design Report (TDR), DESY-01-011, 2001.

[3] A possibility that in realistic non-ideal conditions the photon loads on the TESLA septum and other beamline elements may significantly increase was suggested by Witold Kozanecki in April 2002 based on the talk by Rainer Pitthan in October of 2001.

[4] Andrei Seryi, "Photon Load on the TESLA Extraction Septum Blade", internal ILC-TRC note, July 16, 2002.

[5] Daniel Schulte, "Beam-beam simulations with GUINEA-PIG", ICAP 1998 and CERN-PS-99-014 (LP).

[6] P. Tenenbaum, L. Hendrickson, A. Seryi and G. Stupakov, "Recent Developments in the LIAR Simulation Code", SLAC-PUB-9263, in Proceedings of EPAC 2002.

[7] P. Chen, "Beam-Beam Effects in Linear Colliders", in Handbook on Accelerator Physics and Engineering, World Scientific, 1998, p. 140.

[8] Peter Tenenbaum, "Collimator wakefield calculations for ilc-trc report", LCC-Note-0101, 2002, http://www-project.slac.stanford.edu/lc/ilc/TechNotes/LCCNotes/lcc_notes_index.htm

[9] Glen White, "Beam dynamics simulations, banana bunches, and IP feedback systems", 26th Advanced ICFA Beam Dynamics Workshop on Nanometre-Size Colliding Beams, September 2-6, 2002, Lausanne, http://icfa-nanobeam.web.cern.ch/

[10] L.Hendrickson, T.Raubenheimer, D.Schulte, A.Seryi, P.Tenenbaum, M.Woodley, "Effects of Dynamic Misalignments and Feedback Performance on Luminosity Stability in Linear Colliders", to be published.

[11] L.Hendrickson, T.Raubenheimer, D.Schulte, A.Seryi, P.Tenenbaum, M.Woodley, "Implementation of Dynamic Misalignments and Luminosity Stabilization by Beam-Beam Feedbacks in Simulations of Linear Colliders", to be published.

Figures for Case 1

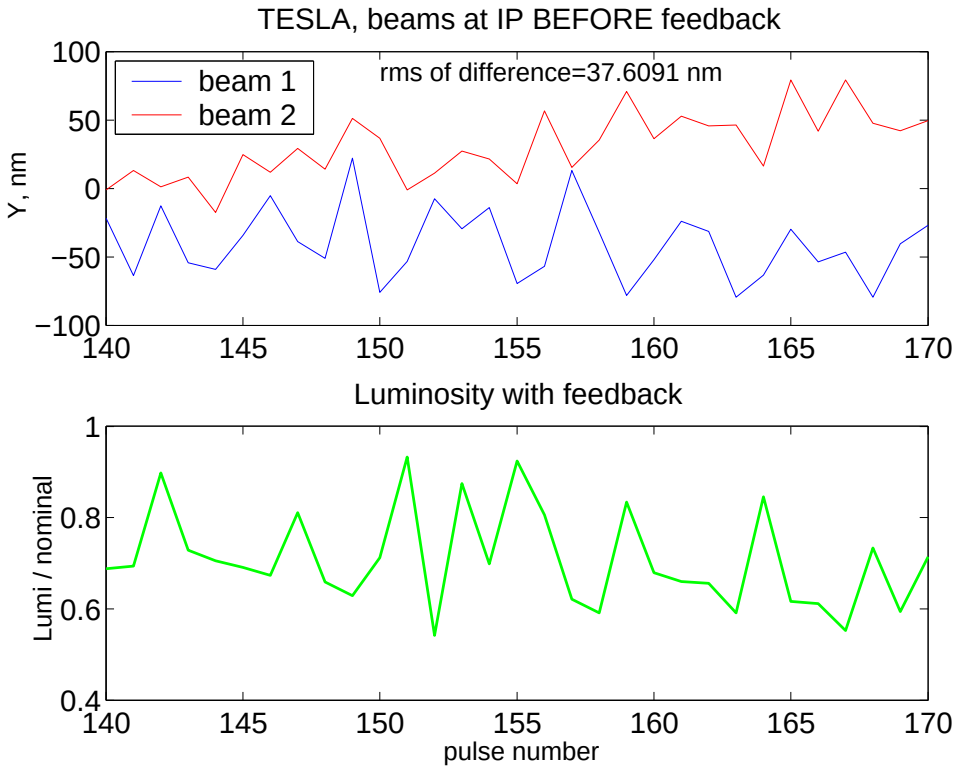

Figure 12: Positions of the beams at the IP before idealized IP feedback is applied versus pulse number (at 5 Hz), top plot. Luminosity versus pulse number with simplified intratrain IP feedback (average X and Y offsets are removed before collision), bottom plot.

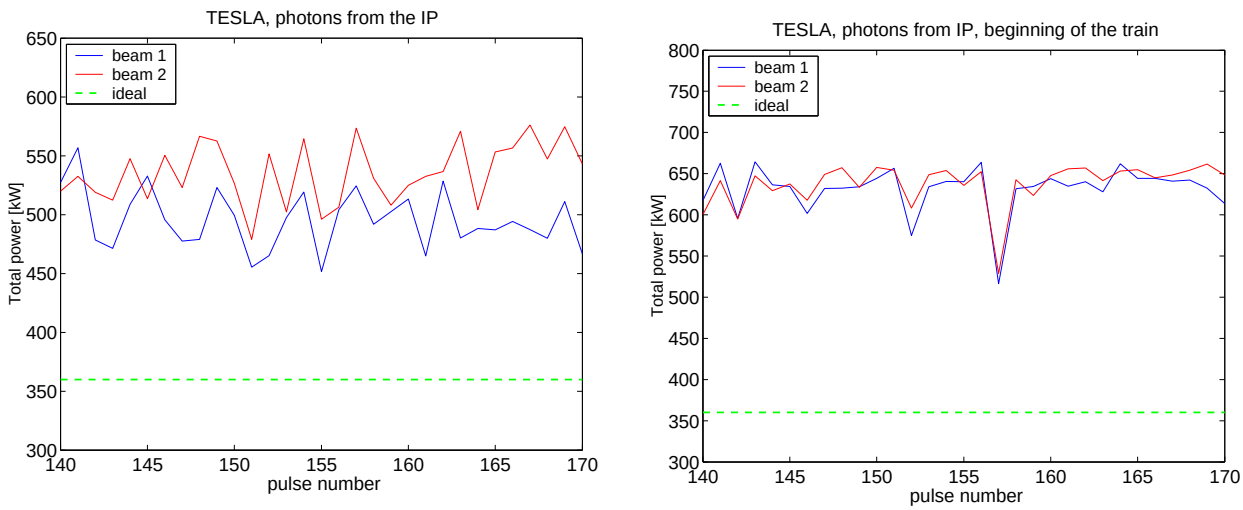

Figure 13: Total power of beamstrahlung photons for the ideal beam and for the non-ideal beam brought into collision by idealized feedback, left plot. Total power of beamstrahlung photons for the non-ideal beam not brought into collision, right plot.

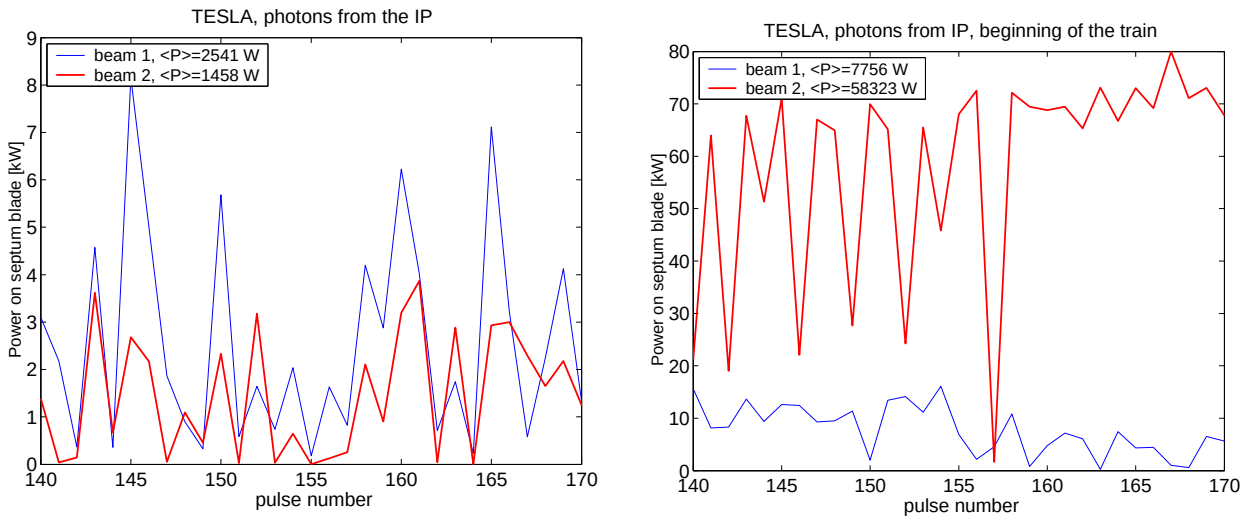

Figure 14: Power of beamstrahlung photons hitting the blade of the septum. Left plot: for the non-ideal beam already brought into collision. Right plot: for the non-ideal beam not yet brought into collision (in this case the losses on the blade should be weighted by the fraction of pulses before the feedback would bring the beams into collision).

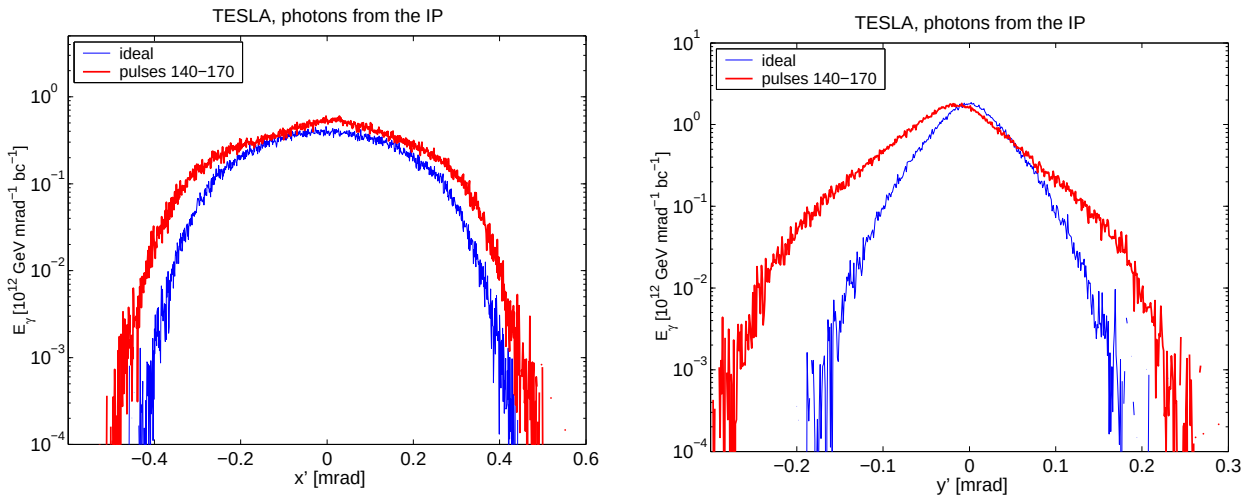

Figure 15: Horizontal (left) and vertical (right) distributions of beamstrahlung photons for the ideal beam and for the non-ideal beam after being brought into collision (average for pulses 140-170).

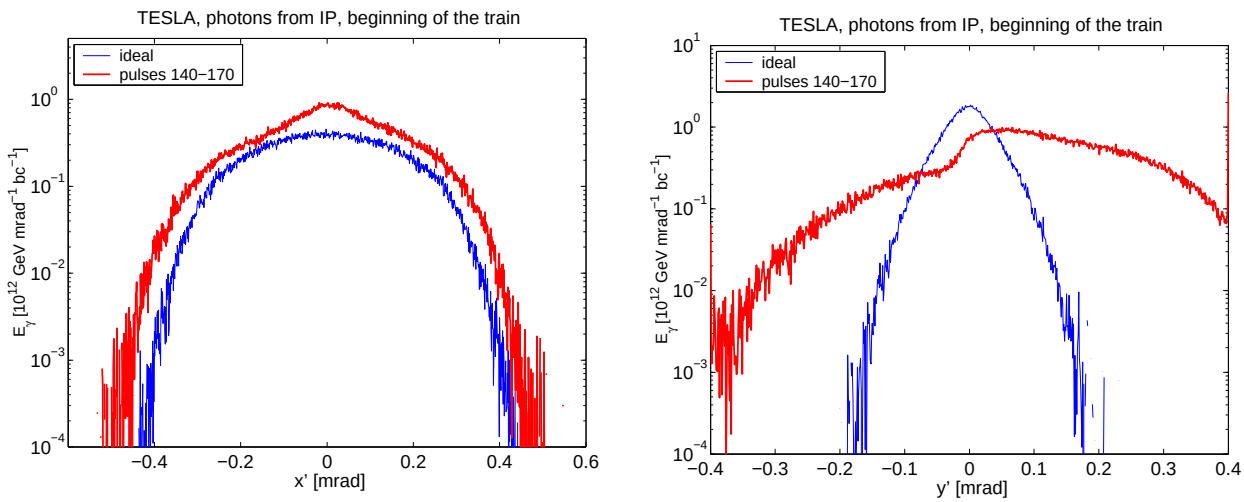

Figure 16: Horizontal (left) and vertical (right) distributions of beamstrahlung photons for the ideal beam and for the non-ideal jittering beam not yet brought into collision (average for pulses 140-170).

Figures for Case 2a

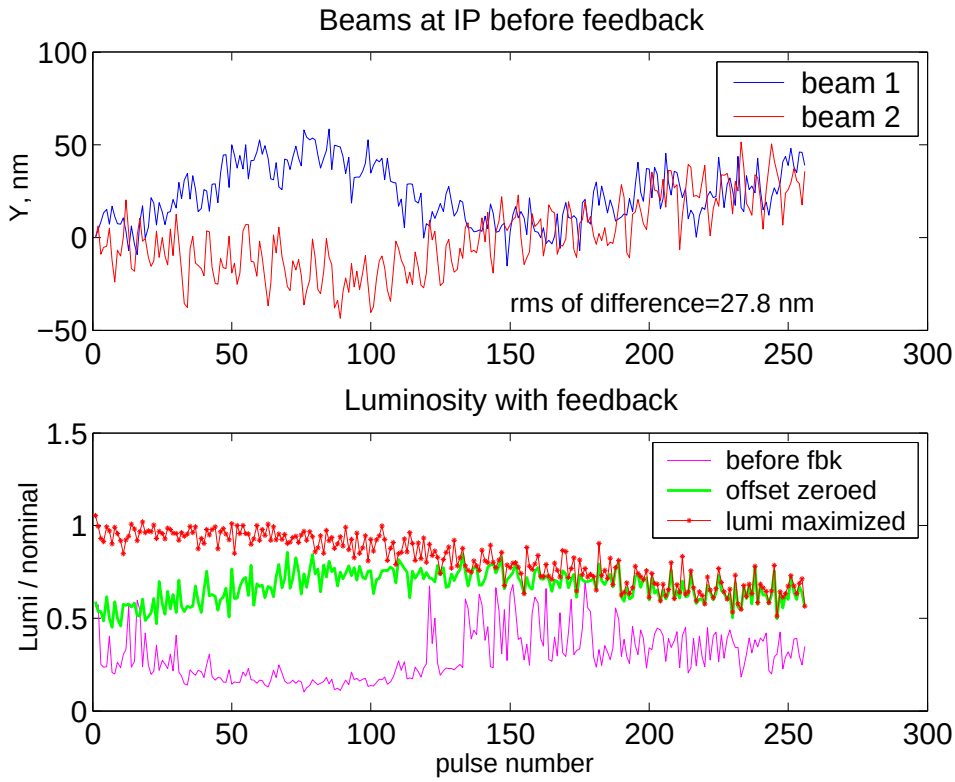

Figure 17: Positions of the beams at IP before idealized IP feedback is applied versus pulse number, top plot. Luminosity versus pulse number before any feedback, after simplified intratrain IP feedback (average X and Y offsets are removed before collision), and after intratrain IP feedback with full optimization (Y and Y' adjusted to maximize luminosity), bottom plot.

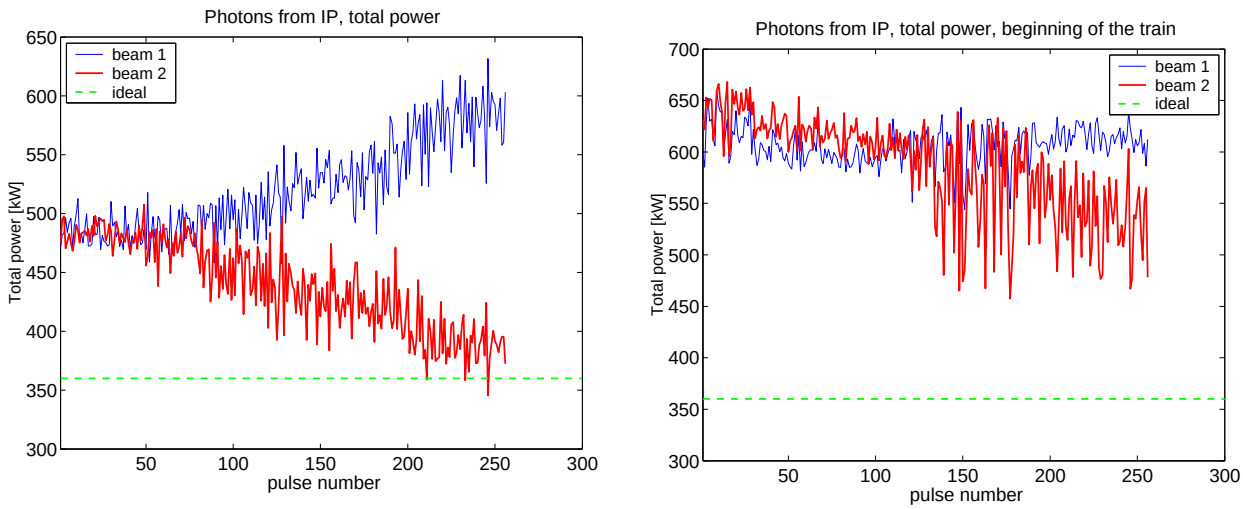

Figure 18: Total power of beamstrahlung photons for the ideal beam and for the non-ideal beam brought into collision by feedback with full optimization, left plot. Total power of beamstrahlung photons for the non-ideal beam not brought into collision, right plot.

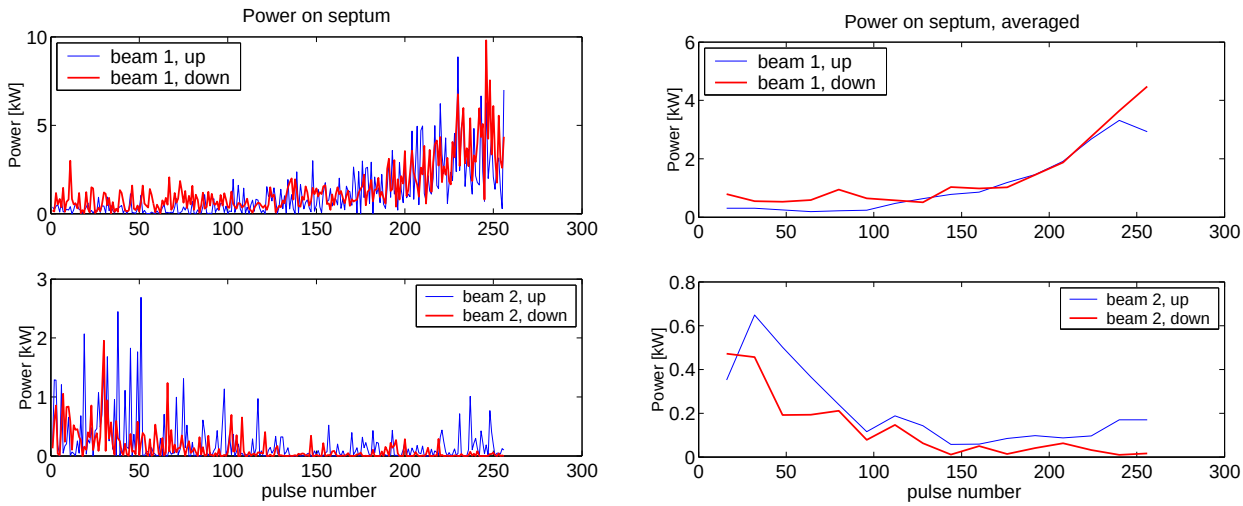

Figure 19: Power of beamstrahlung photons hitting the blade of the septum for the non-ideal beam after being brought into collision by feedback with full optimization (left plot). Right plot show the same power averaged over 16 pulses.

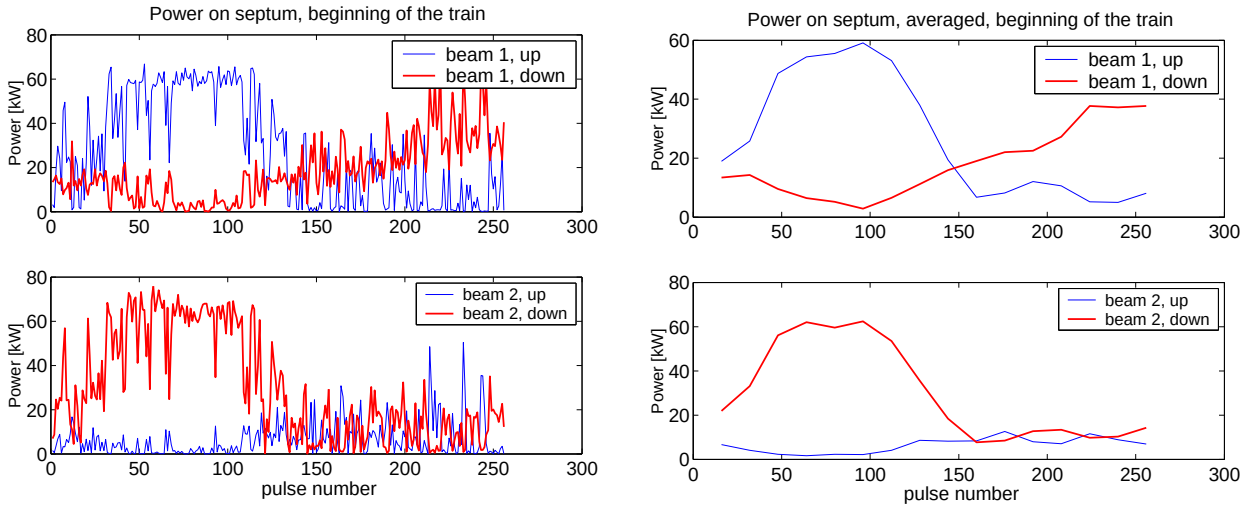

Figure 20: Power of beamstrahlung photons hitting the blade of the septum for the non-ideal beam not yet brought into collision (in this case the losses on the blade should be weighted taking into account how fast the feedback would bring the beams into collision).

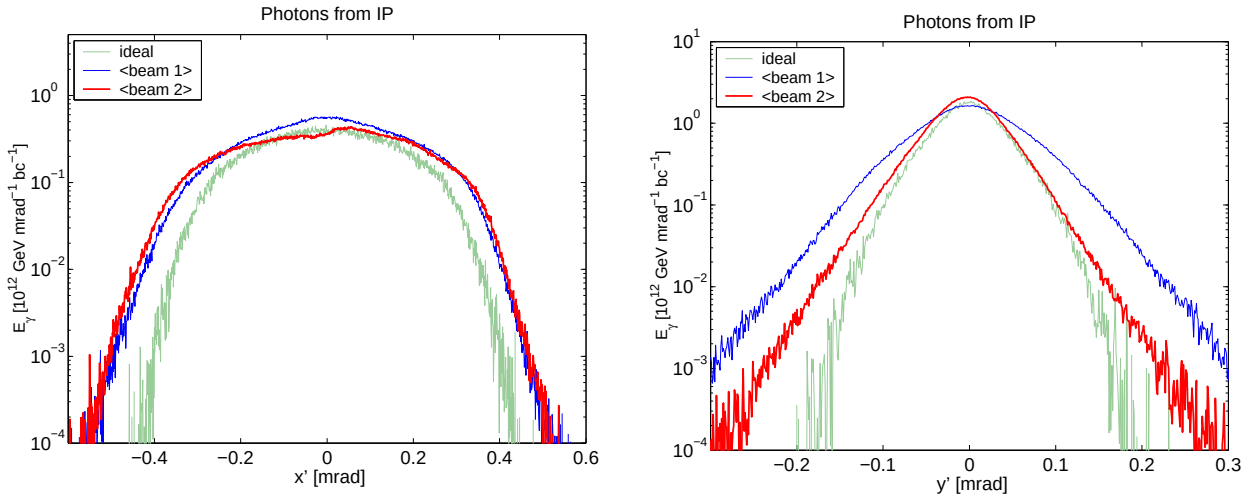

Figure 21: Horizontal (left) and vertical (right) distributions of beamstrahlung photons for the ideal beam and for the non-ideal beam after being brought into collision (average for pulses 1-256).

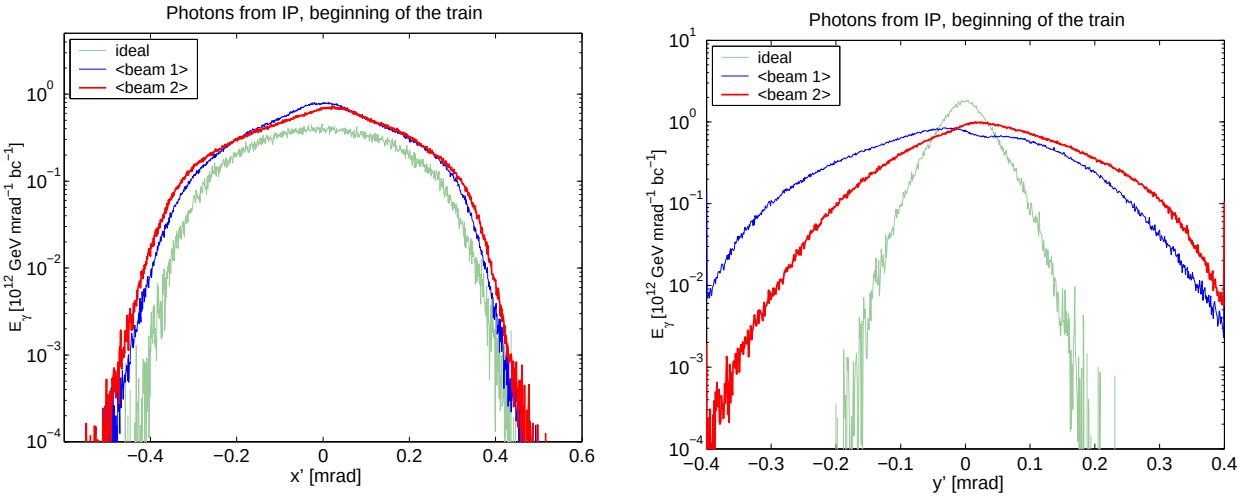

Figure 22: Horizontal (left) and vertical (right) distributions of beamstrahlung photons for the ideal beam and for the non-ideal jittering beam not yet brought into collision (average for pulses 1-256).

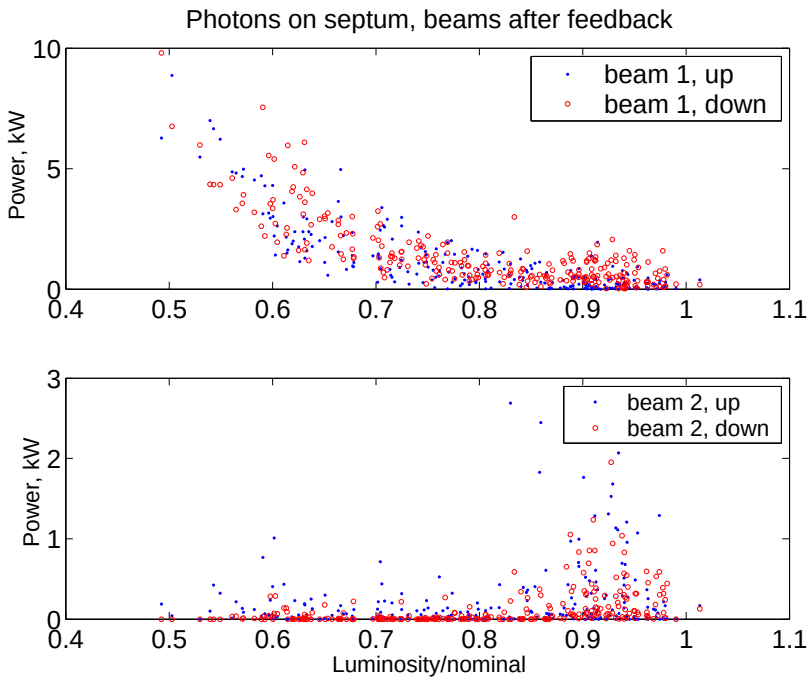

Figure 23: Power on the septum blade versus luminosity for the beams after being brought into collision by feedback with full optimization (pulses 1-256).

Figures for Case 2b

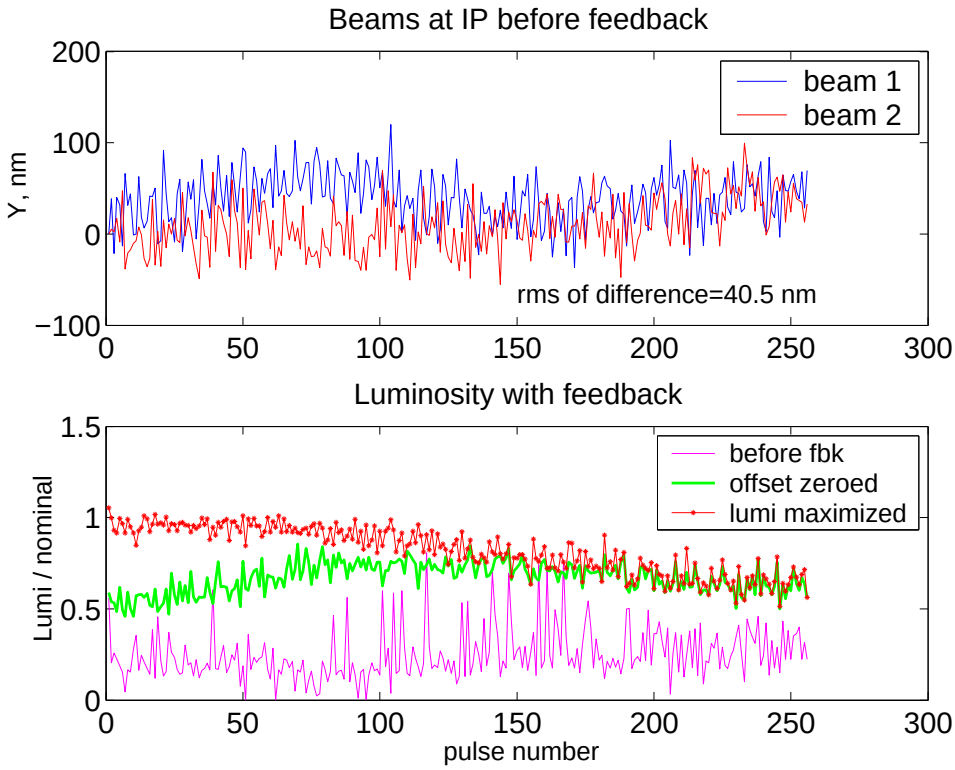

Figure 24: Positions of the beams at IP before idealized IP feedback is applied versus pulse number, top plot. Luminosity versus pulse number before any feedback, after simplified intratrain IP feedback (average X and Y offsets are removed before collision), and after intratrain IP feedback with full optimization (Y and Y' adjusted to maximize luminosity), bottom plot.

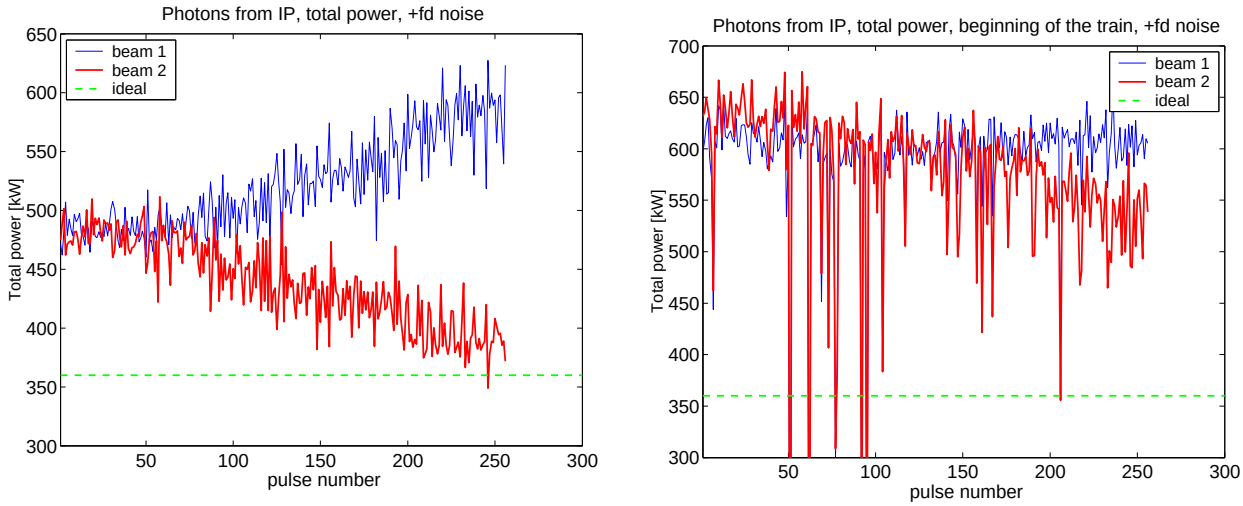

Figure 25: Total power of beamstrahlung photons for the ideal beam and for the non-ideal beam brought into collision by feedback with full optimization, left plot. Total power of beamstrahlung photons for the non-ideal beam not brought into collision, right plot.

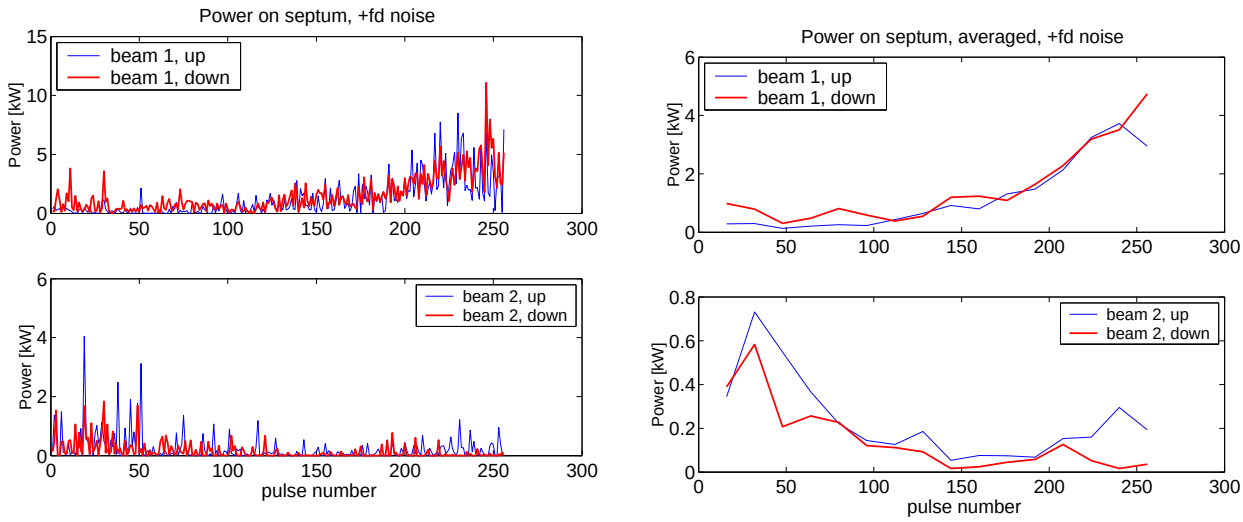

Figure 26: Power of beamstrahlung photons hitting the blade of the septum for the non-ideal beam after being brought into collision by feedback with full optimization (left plot). Right plot show the same power averaged over 16 pulses.

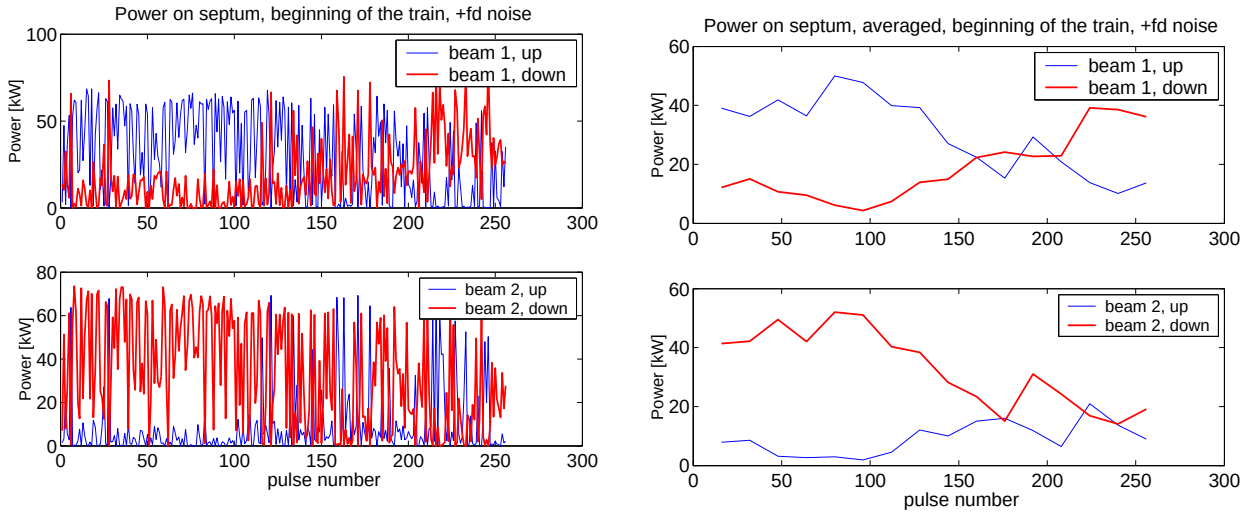

Figure 27: Power of beamstrahlung photons hitting the blade of the septum for the non-ideal beam not yet brought into collision (in this case the losses on the blade should be weighted taking into account how fast the feedback would bring the beams into collision).

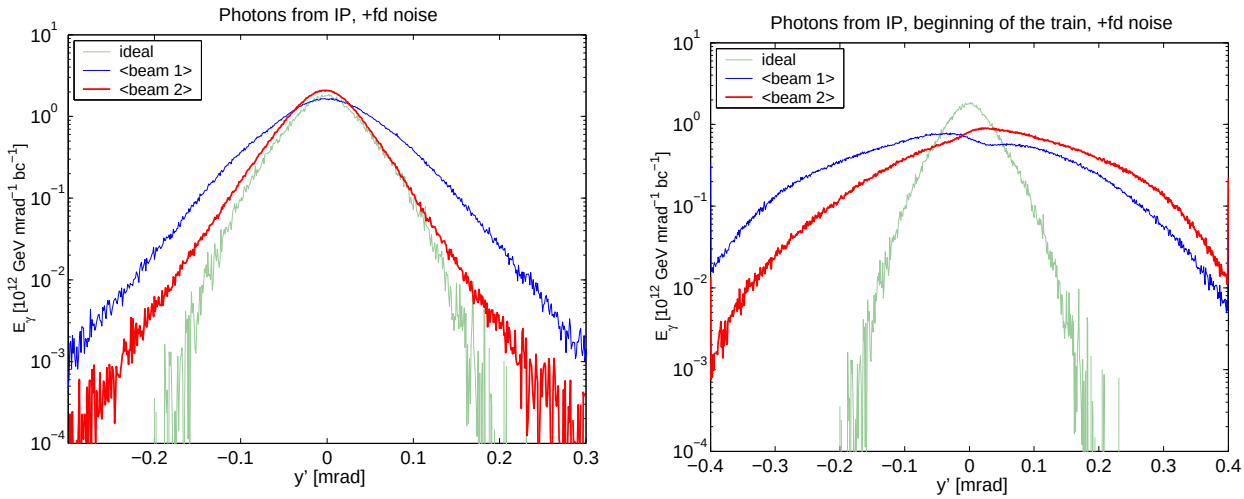

Figure 28: Vertical distribution of beamstrahlung photons for the ideal beam, for the non-ideal beam after being brought into collision (left plot) and for the non-ideal jittering beam not yet brought into collision (right plot), average for pulses 1-256.

Figures for Case 3a

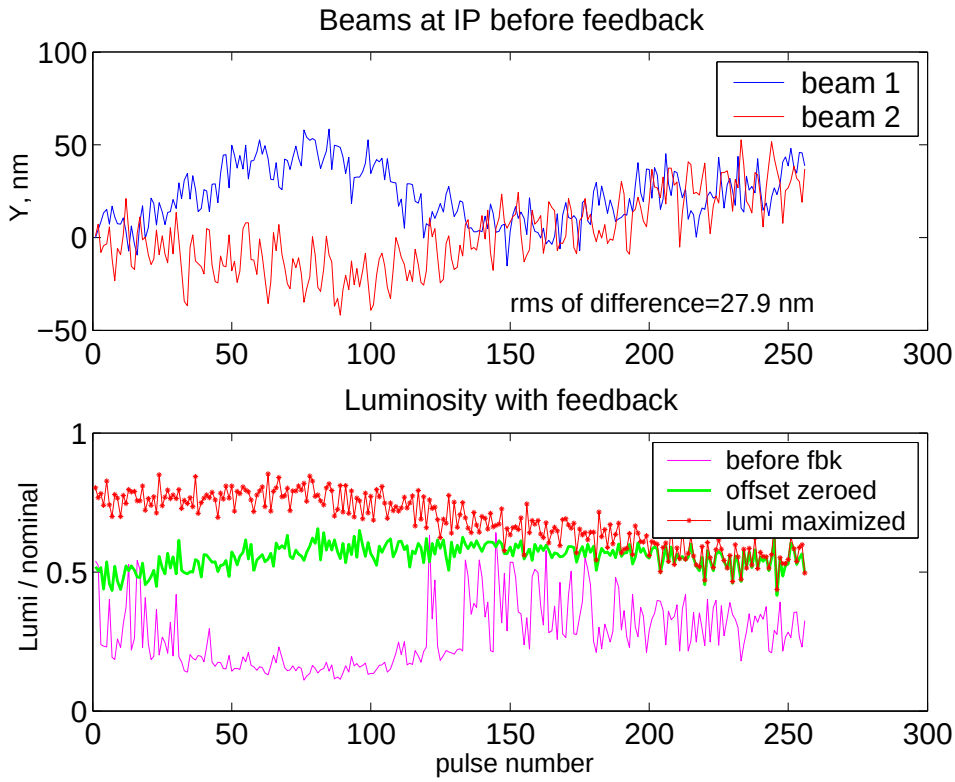

Figure 29: Positions of the beams at IP before idealized IP feedback is applied versus pulse number, top plot. Luminosity versus pulse number before any feedback, after simplified intratrain IP feedback (average X and Y offsets are removed before collision), and after intratrain IP feedback with full optimization (Y and Y' adjusted to maximize luminosity), bottom plot.

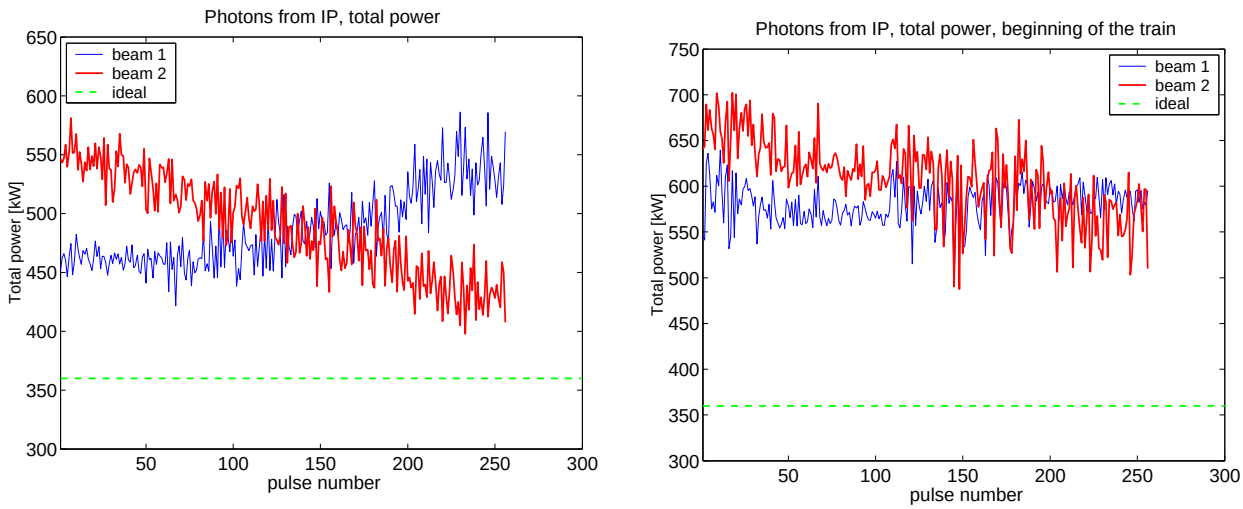

Figure 30: Total power of beamstrahlung photons for the ideal beam and for the non-ideal beam brought into collision by feedback with full optimization, left plot. Total power of beamstrahlung photons for the non-ideal beam not brought into collision, right plot.

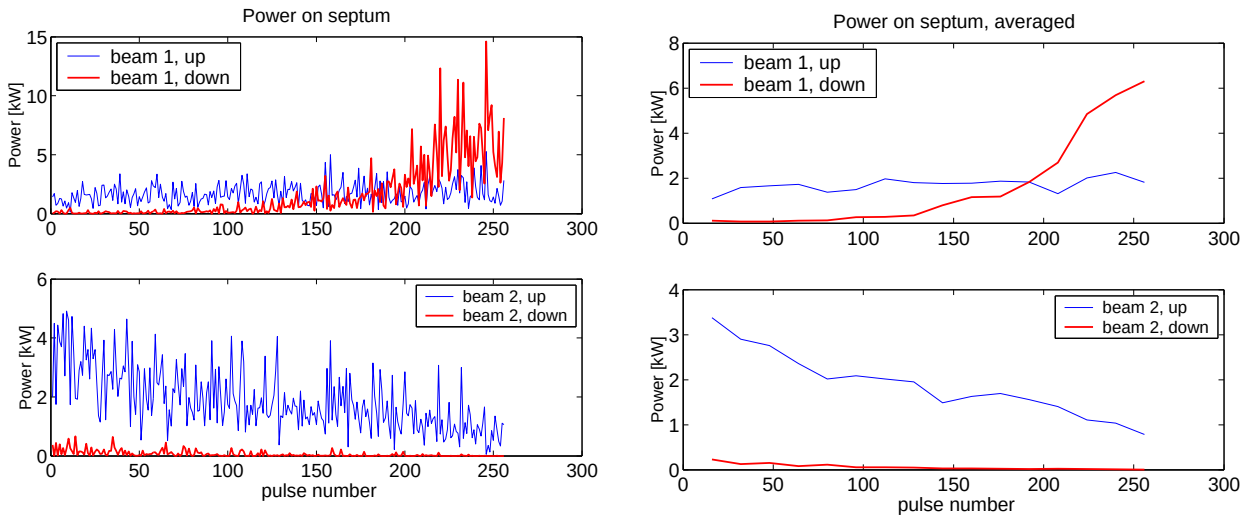

Figure 31: Power of beamstrahlung photons hitting the blade of the septum for the non-ideal beam after being brought into collision by feedback with full optimization (left plot). Right plot show the same power averaged over 16 pulses.

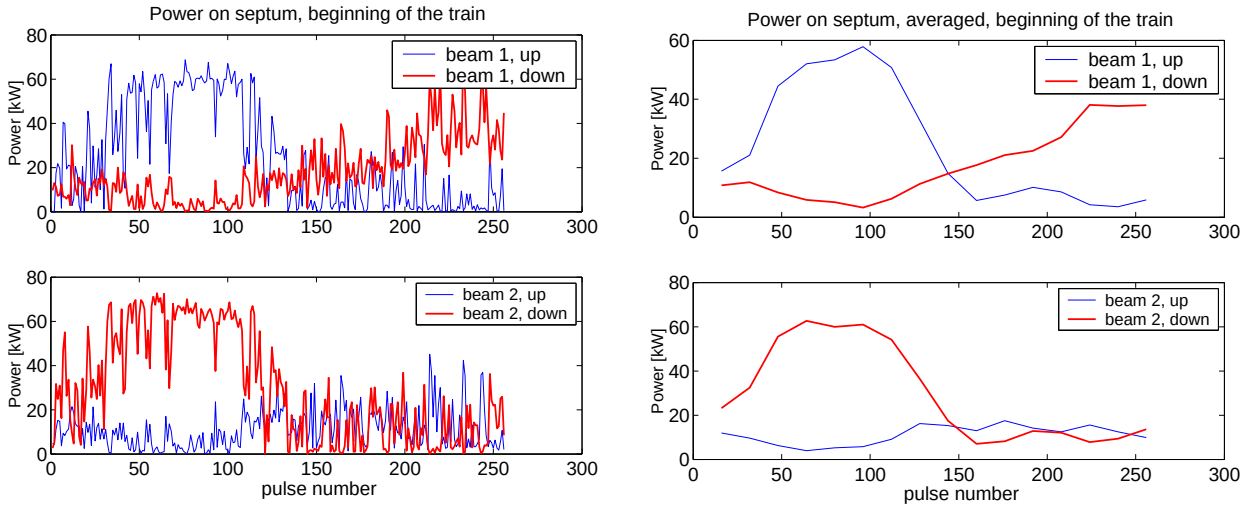

Figure 32: Power of beamstrahlung photons hitting the blade of the septum for the non-ideal beam not yet brought into collision (in this case the losses on the blade should be weighted taking into account how fast the feedback would bring the beams into collision).

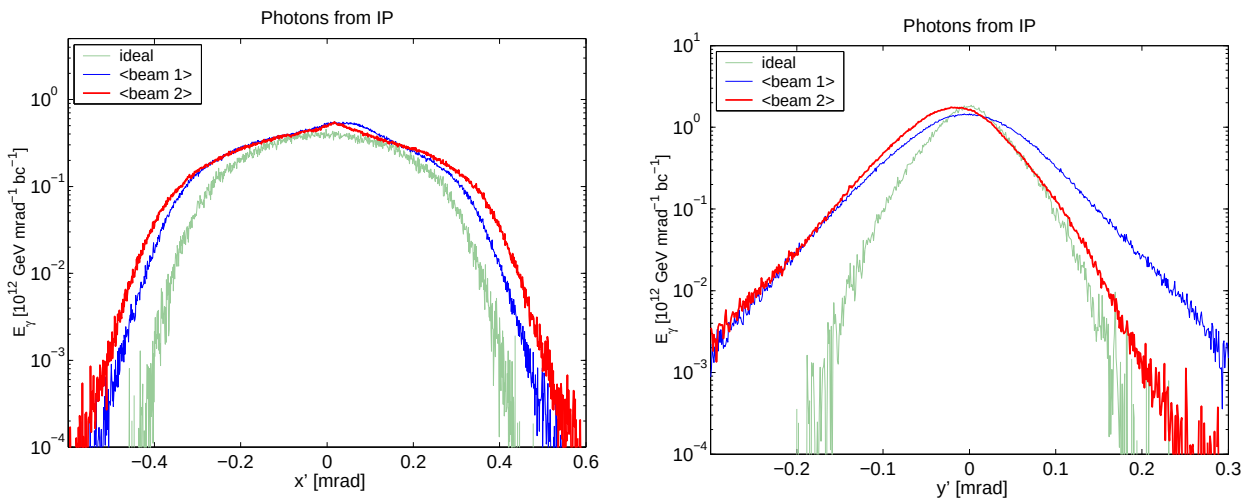

Figure 33: Horizontal (left) and vertical (right) distributions of beamstrahlung photons for the ideal beam and for the non-ideal beam after being brought into collision (average for pulses 1-256).

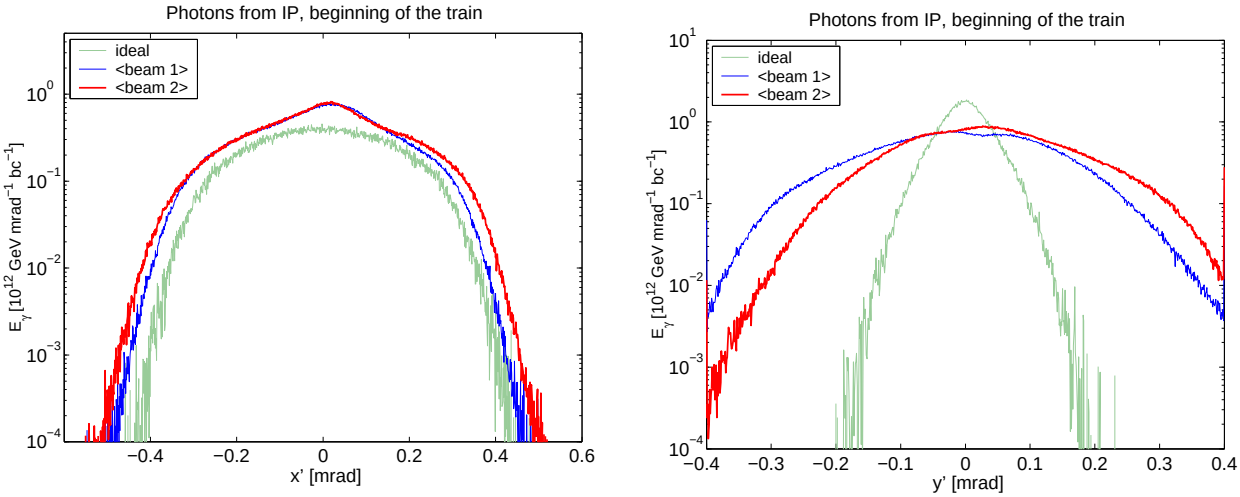

Figure 34: Horizontal (left) and vertical (right) distributions of beamstrahlung photons for the ideal beam and for the non-ideal jittering beam not yet brought into collision (average for pulses 1-256).

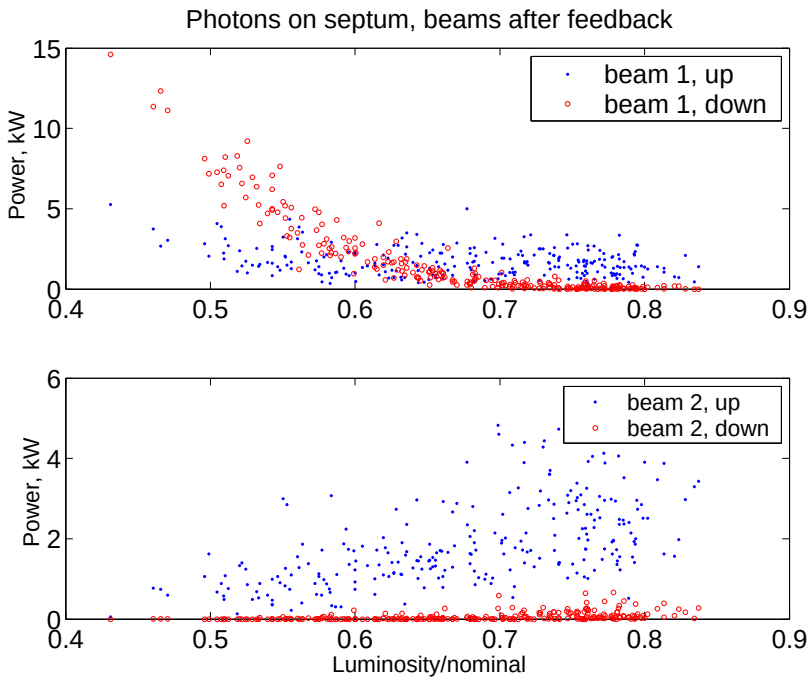

Figure 35: Power on the septum blade versus luminosity for the beams after being brought into collision by feedback with full optimization (pulses 1-256).

Figures for Case 3b

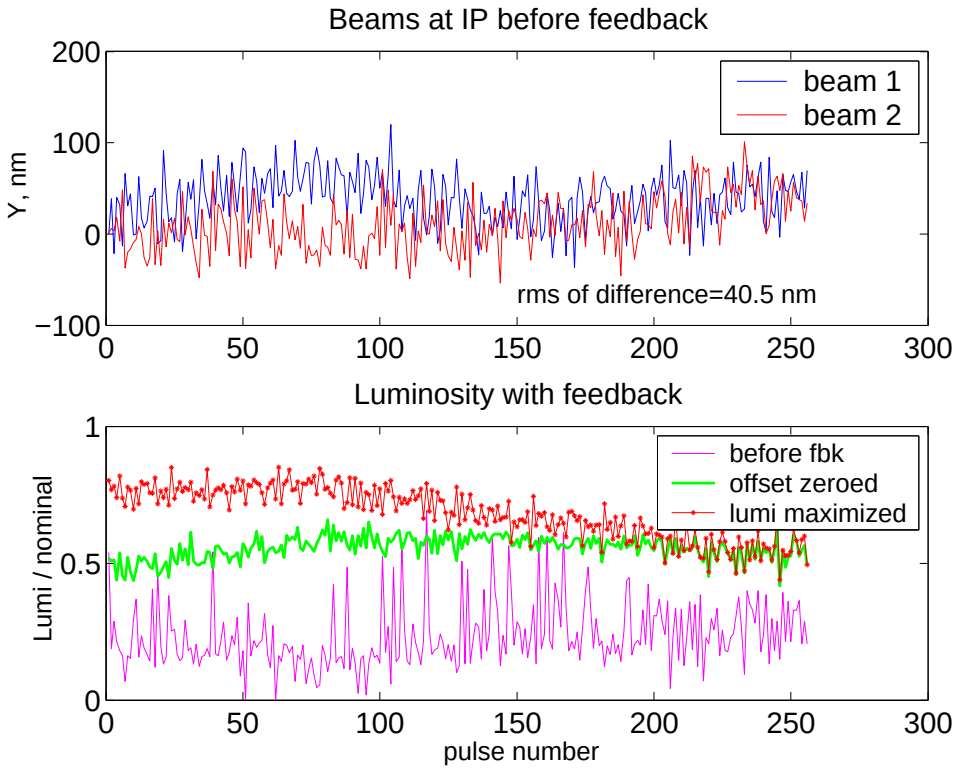

Figure 36: Positions of the beams at IP before idealized IP feedback is applied versus pulse number, top plot. Luminosity versus pulse number before any feedback, after simplified intratrain IP feedback (average X and Y offsets are removed before collision), and after intratrain IP feedback with full optimization (Y and Y' adjusted to maximize luminosity), bottom plot.

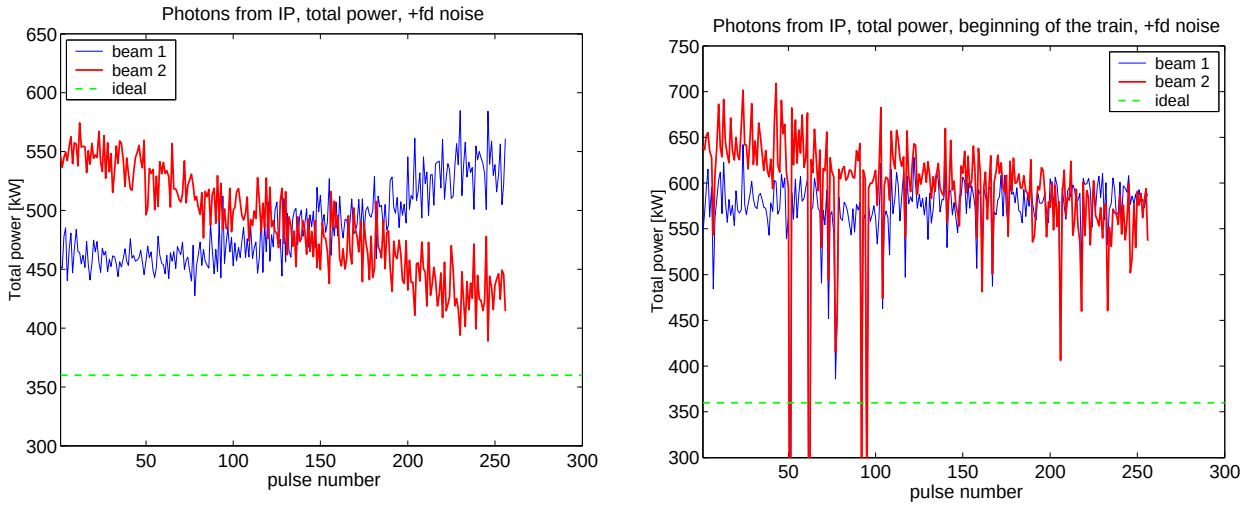

Figure 37: Total power of beamstrahlung photons for the ideal beam and for the non-ideal beam brought into collision by feedback with full optimization, left plot. Total power of beamstrahlung photons for the non-ideal beam not brought into collision.

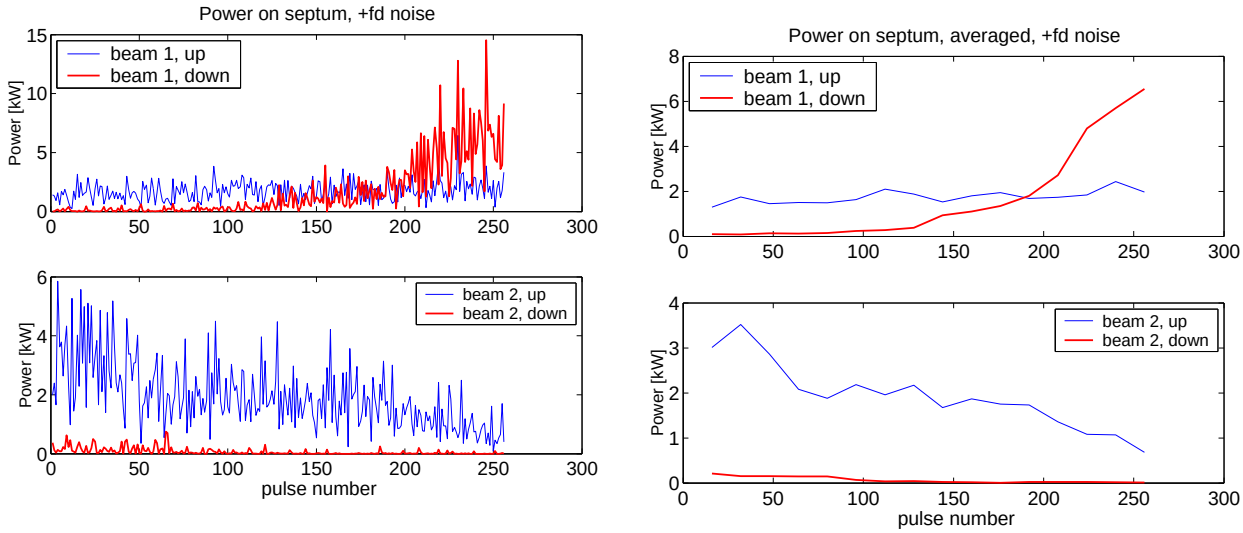

Figure 38: Power of beamstrahlung photons hitting the blade of the septum for the non-ideal beam after being brought into collision by feedback with full optimization (left plot). Right plot show the same power averaged over 16 pulses.

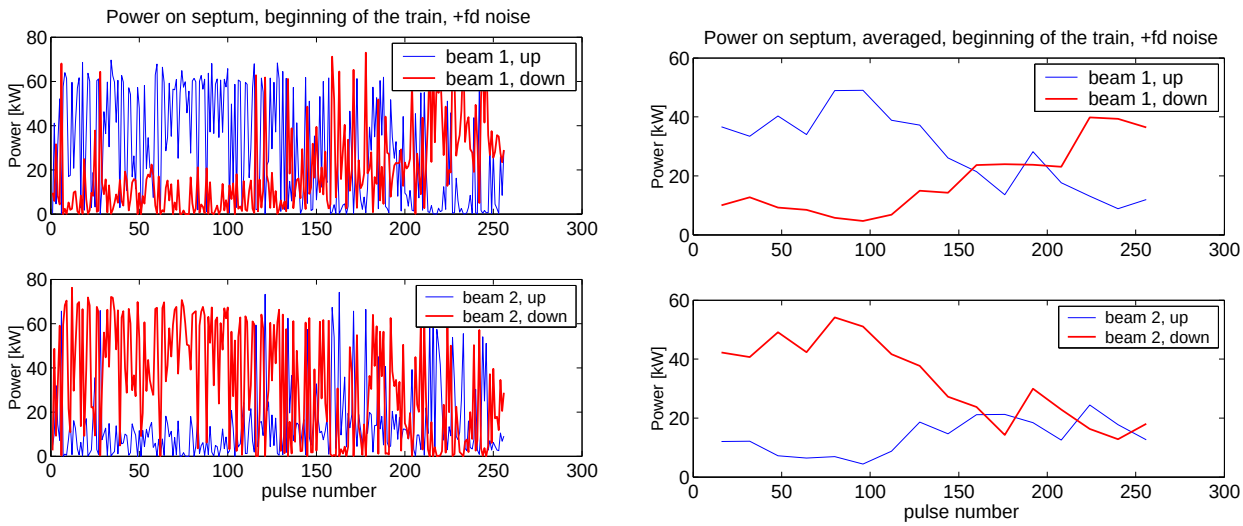

Figure 39: Power of beamstrahlung photons hitting the blade of the septum for the non-ideal beam not yet brought into collision (in this case the losses on the blade should be weighted taking into account how fast the feedback would bring the beams into collision).

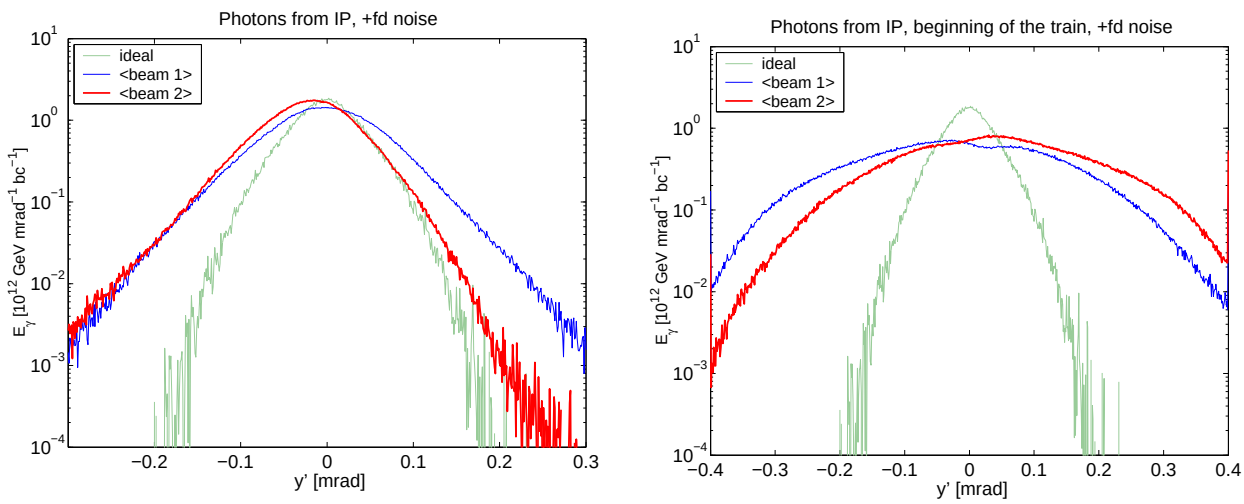

Figure 40: Vertical distribution of beamstrahlung photons for the ideal beam, for the non-ideal beam after being brought into collision (left plot) and for the non-ideal jittering beam not yet brought into collision (right plot), average for pulses 1-256.